TABLE 1. Primers for the *MET*, $p16^{INK4A}$, and $p14^{ARF}$ Genes for PCR-SSCP

Exon	Primer sequence (5′→3′) Forward	Reverse
MET[a]		
14	CCATGATAGCCGTCTTTAAC	ATACTTACTTGGCAGAGGT
15	GTCCCCATTAAATGAGGTTT	ATCTGCAAAGGCCAAAGATA
16	ATGTTACGCAGTGCTAACC	GTAGCTGATTTTTCCACAAG
17	GAAGTTAATGTCTCCACCAC	TGGCTTACAGCTAGTTTGCC
18	TTCTAACTCTCTTTGACTGC	CAGATTCCTCCTTGTCACTT
19	ATTCTATTTCAGCCACGGG	AGGAGAAACTCAGAGATAACC
20	ACCTCATCTGTCCTGTTTC	CCAAAAAGAAAGACATGCTG
21	GGGTCTCTTACAGCATGTCT	GTGTGGACTGTTGCTTTGAC
$p16^{b}$		
1	GCTGCGGAGAGGGGGAGAGCAGGCA	CTGCAAACTTCGTCCTCCA
2-1	CTTCCTTTCCGTCATGCCG	CTCAGCCAGGTCCACGGGCA
2-2	TTCCTGGACACGCTGGTGGTG	GGAAGCTCTCAGGGTACAAA
3	TGCCACACATCTTTGACCTC	AAAACTACGAAAGCGGGGTG
$p14^{b}$		
1-1	CGCTCAGGGAAGGCGGGTGC	AACCACGAAAACCCTCACTC
1-2	ATGGTGCGCAGGTTCTTGGT	ACCAAACAAAACAAGTGCCG

[a]GenBank accession number for *MET* is NT_007933.
[b]GenBank accession number for *CDKN2A* is NT_008413.

supplemented with 10% fetal bovine serum in a humidified atmosphere containing 5% CO_2 at 37°C.

Thirty-two primary RMS tumors, obtained at the time of initial surgery or biopsy in several hospitals in Japan (1993–2005), were examined. Histopathological diagnosis was made by pathologists at each hospital. Of the 32 cases (age range, 0–20 years; median age, 5.8 years), 5 were classified as stage I, 5 as II, 10 as III, and 12 as IV, according to the Intergroup Rhabdomyosarcoma Study-IV (IRS-IV) staging classification. Twenty-one cases were ERMS, and 11 were ARMS. Patients with stage I or II were treated with surgery alone or surgery plus chemotherapy, mainly vincristine. Patients with stage III or IV were treated with surgery, radiotherapy, intensive multidrug chemotherapy, and if necessary, autologous bone marrow transplantation.

All of the cell lines and fresh tumors were previously screened for mutations of *TP53*.

Normal human skeletal muscle total RNA was obtained from two healthy patients (aged 3 and 5). Ten peripheral blood (PB) samples from healthy volunteers were also used as normal controls.

Informed consent was obtained from the patients and/or their parents as well as healthy volunteers.

DNA and RNA Preparation

High-molecular-weight DNA was extracted from all samples by proteinase K digestion and phenol/chloroform extraction. Total RNA was extracted from all of the cell lines and 17 fresh tumors using the acid guanidine thiocyanate-phenol chloroform method. Randomly primed cDNA was synthesized from total RNA using a cDNA synthesis kit as previously described (Shibuya et al., 2001).

Mutational Analyses for *MET* and *CDKN2A* in RMS

The mutations of *MET* identified to date are clustered in the transmembrane domain and tyrosine kinase domain (Trusolino and Comoglio, 2002). Therefore, we examined exons 14–21 of *MET*, which encompassed the two domains and the juxtamembrane region, for all of the cell lines and fresh tumors by PCR-single-strand conformation polymorphism (PCR-SSCP) analyses as described elsewhere (Chen et al., 2005). For *CDKN2A*, we screened its whole coding region by PCR-SSCP. The primers for PCR-SSCP are listed in Table 1. For samples that showed altered mobility, we subjected the PCR products to direct sequencing analyses (Chen et al., 2005, 2006). Furthermore, we performed another round of direct sequence analyses in all cell lines for *MET* and *CDKN2A* to verify the results of PCR-SSCP.

Real-Time Quantitative PCR

For seven RMS cell lines and 17 fresh tumors, real-time quantitative PCR (RQ-PCR) analyses were carried out to quantify the expression levels of *MET*, $p16^{INK4A}$ and $p14^{ARF}$, using a QuantiTect™ SYBR Green PCR Kit (Qiagen, Tokyo,

Japan) with an iCycler iQ™ real-time PCR detection system (Bio-Rad Japan, Tokyo, Japan). The reaction mixture was prepared as follows: 1 μl of cDNA, 1×QuantiTect SYBR Green PCR Master Mix, 0.3 μm of each primer and 0.5 U of uracil-*N*-glycosylase (Applied Biosystems, Tokyo, Japan) in a final volume of 50 μl. The amplification conditions for quantitation were an initial 2 min of incubation at 50°C, 15 min at 95°C, followed by 40 cycles of amplification (denaturation at 95°C for 30 sec, annealing at the respective temperatures for 30 sec, extension at 72°C for 30 sec) (Chen et al., 2003). The primer sets used for real-time quantitative reverse transcriptase-PCR were as follows: sense 5′-GGTTGCTGATTTTGGTCTTG-3′ and antisense 5′-GCAGTATTCGGGTTGTAGGA-3′ for *MET* (GenBank accession number NM_000245); sense 5′-GCCCAACGCACCGAATAG-3′ for $p16^{INK4A}$ (GenBank accession number NM_058197), 5′-TCTGGTTCTTTCAATCGGGGA-3′ for $p14^{ARF}$ (GenBank accession number NM_058195) and the same antisense 5′-ACCACCAG-CGTGTCCAGGAA-3′ for $p16^{INK4A}$ or $p14^{ARF}$. The β-*actin* gene served as an endogenous control. The primers for β-*actin* amplification were sense 5′-CTTCTACAATGAGCTGCGTG-3′ and antisense 5′-TCATGAGGTAGTCAGTCAGG-3′. For the purpose of normalization, the relative expression level was calculated by dividing the expression level of the respective gene by that of the β-*actin* gene for each sample.

For the seven RMS cell lines and 17 fresh tumors, the relative DNA copy number of *MET* or *CDKN2A* in each sample was quantified using RQ-PCR analyses similar to above. Each DNA sample had an $A_{260/280}$ ratio in the range 1.60–1.80 and was diluted to 100 ng/μl before use. The primer set for *MET* was that for mutational screening of exon 16 and the primer set for *CDKN2A* was that for mutational screening of the common exon 2, respectively (Table 1). The *B2M* (β-2-microglobulin) gene, which was a housekeeping gene on chromosome 15q21-q22.2 (Lillington et al., 2002), was used as an endogenous reference and the copy number of *MET* as well as *CDKN2A* in each sample was normalized by the corresponding *B2M* value. The primers for *B2M* amplification were sense 5′-AAGTGGAGCATTCAGACTTG-3′ and antisense 5′-TCCCTGACAATCCCAATATG-3′ (GenBank accession number NT_010194).

All of the reactions were run in triplicate. The primers used for RT-PCR were designed to prevent DNA amplification, and the melting curve was incorporated to detect whether primer dimers or other undesired products were amplified. In addition, all of the amplified products were subjected to gel electrophoresis, and if necessary, direct sequence analysis was performed to confirm the expected PCR products.

Detection of *PAX3-FKHR* and *PAX7-FKHR* Chimeric Transcripts

For the seven RMS cell lines and 17 fresh tumors, we also examined the expression of *PAX3-FKHR* and *PAX7-FKHR* chimeric transcripts as described previously (Galili et al., 1993; Davis et al., 1994).

Western Blotting and Immunoprecipitation Analyses

Rabbit polyclonal antibodies against human MET (C-12) and mouse monoclonal antibodies against phosphorylated tyrosine (p-Tyr) (PY99) were purchased from Santa Cruz Biotechnology (Santa Cruz, CA). The secondary antibodies (donkey anti-rabbit IgG and sheep anti-mouse IgG conjugated with horseradish peroxidase) and enhanced chemiluminescence reagent were purchased form Amersham Biosciences (Piscataway, NJ). Total cellular proteins were extracted by lysing 1×10^6 cells with a lysis buffer [50 mM HEPES-NaOH (pH7.0), 1% NP40, 1% sodium deoxycholate, 0.1% sodium dodecyl sulfate (SDS), 250 mM NaCl, 5 mM NaF, 1 mM DTT, 1 mM phenylmethylsulfonyl fluoride, and 50 μg/ml aprotinin] from 7 RMS cell lines (Takita et al., 1997). The proteins were separated by SDS-PAGE by loading the lysates containing 50 μg of total protein on a 4–20% gradient gel, and then transferring onto a polyvinylidene difluoride transfer membrane (Millipore, Billerica, MA) (Takita et al., 1997). The membranes were incubated with the anti-MET antibody, followed by the HRP-conjugated secondary antibody. The resultant immunoproducts were detected with the ECL Western Blotting Analysis System. Equal protein loading was confirmed by staining the membrane with Coomassie brilliant blue. The Western blotting analysis for MET was performed three times, then the blots were scanned, and the level of MET in each sample was estimated using the NIH Image 1.61 software (Wayne Rasband, National Institutes of Health, MD). The protein expression level of each cell line was calculated as mean ± SD.

For immunoprecipitation (IP), lysates containing 500 μg of total protein were pretreated with 1 μg of normal rabbit IgG and 20 μl of protein G-plus

TABLE 2. Expression of *MET*, $p16^{INK4A}/p14^{ARF}$, and *PAX3-FOXO1A* Transcript, and Mutations of *TP53* in RMS Cell Lines

		MET		*p16*	*p14*		
Cell lines	Histology	mRNA[a]	Protein[a]	mRNA	mRNA	*PAX3-FOXO1A*	Mutation of *TP53*
SJRH-1	E	13.06 ± 0.50	11.78 ± 8.08	0.03 ± 0.00	0.74 ± 0.12	−	Tyr220Cys
SJRH-4	A	122.99 ± 30.86	71.35 ± 37.72	0.73 ± 0.02	0.96 ± 0.22	+	13bp del[b]
SJRH-18	A	59.70 ± 13.07	60.12 ± 21.94	0.13 ± 0.08	0.38 ± 0.11	+	Gly187Cys
SJRH-30	A	363.04 ± 54.41	166.35 ± 61.83	0.92 ± 0.01	1.19 ± 0.02	+	Tyr205Cys
RD	E	28.13 ± 7.14	22.45 ± 7.05	0.16 ± 0.03	0.90 ± 0.04	−	Arg248Trp
RMS	E	8.17 ± 0.74	14.66 ± 6.61	0.49 ± 0.07	0.97 ± 0.03	−	Arg282Trp[c]
SCMC-RM2	A	155.08 ± 29.28	109.50 ± 62.99	0.55 ± 0.03	1.05 ± 0.07	+	−

E, embryonal type; A, alveolar type.
[a]The values for mRNA and protein indicate mean ± SD.
[b]Nucleotide 701–713 (GenBank accession number for *TP53* is NM_000546).
[c]Single nucleotide polymorphism (SNP). GenBank accession number for Arg282Trp is rs28934574.

agarose beads (Santa Cruz, CA) at 4°C for 30 min. After removal of the beads by centrifugation, lysates were incubated with the anti-MET antibody (2 μg) and 20 μl of protein G-plus agarose beads overnight at 4°C. The immunoprecipitates were washed three times with PBS/0.1%NP-40 and resuspended in lysis buffer, followed by Western blot analyses as described above with anti-p-Tyr (PY99). Then, the antibodies were stripped from the membrane in a stripping buffer containing 62.5 mmol/l Tris, 2% SDS, and 100 mmol/l β-mercaptoethanol. The membrane was reprobed with C-12 and the relative secondary antibodies to confirm the expression of MET.

Statistical Analyses

The Mann-Whitney *U* test was used to compare the expression level of each gene between subgroups of RMS. Fisher's exact test was used to evaluate the statistical significance of differences in proportions among groups. Kaplan–Meier survival plots were constructed, and log-rank tests were used to estimate survival. Exact 95% CI of proportions were calculated on the basis of binomial distribution. The Spearman rank correlation was calculated to evaluate the correlation between the mRNA expression and protein expression of MET. Two-sided $P < 0.05$ was required for significance. All analyses were carried out with StatView-J 4.5software (Abacus Concepts, CA).

RESULTS

Mutations of *MET* and *CDKN2A* in RMS

For seven cell lines and 32 fresh tumors of RMS, no mutations (0.0%; 95% CI, 0.0–9.0%) were detected in exons 14–21 of *MET* by PCR-SSCP. For *CDKN2A*, one nonsense mutation (CGA > TGA) (2.6%; 95% CI, 0.5–13.2%), resulting in a truncated protein at codon 80 of $p16^{INK4A}$, was observed in an ARMS cell line, SJRH-18. The same mutation was reported previously in melanoma (Orlow et al., 2001). This C > T transition also results in a missense mutation (Pro135Leu) in $p14^{ARF}$. A polymorphism (Ala148Thr) in $p16^{INK4A}$ was detected in another ARMS cell line, SJRH-30. No mutations of $p16^{INK4A}$ or $p14^{ARF}$ were identified in the 32 fresh tumors.

Expression of *MET* and $p16^{INK4A}/p14^{ARF}$ mRNA in RMS

Using RQ-PCR, the expression of *MET* was detected in all of the RMS samples and normal skeletal muscles. The *MET*/β-*actin* value in RMS ranged from 6.16 to 424.42, with a mean value of 102.60 ± 124.86, whereas the *MET*/β-*actin* value in normal muscles was 33.20 ± 3.77. Overexpression of *MET* (> mean value), was detected in 7 of 24 RMS samples, which included 3 alveolar cell lines (SJRH-4, SJRH-30, SCMC-RM2) (3/7), and 2 alveolar and 2 embryonal type tumors (4/17) (Table 2 and Fig. 1A).

The $p16^{INK4A}$/β-*actin* value in RMS ranged from 0 to 3.59, with a mean value of 0.74 ± 0.96. Reduced or absent expression of $p16^{INK4A}$ ($p16^{INK4A}$/β-*actin* less than half the mean value) was observed in 11 of 24 samples, which included 3 cell lines (SJRH-1, SJRH-18, RD) and 8 fresh tumors (Table 2).

The $p14^{ARF}$/β-*actin* value in RMS ranged from 0 to 3.53, with a mean value of 0.85 ± 0.94. Reduced or absent expression of $p14^{ARF}$ ($p14^{ARF}$/β-*actin* less than half the mean value) was shown in 10 of 24 samples, which included 1 cell line (SJRH-18) and 9 fresh tumors (Table 2).

Two fresh tumors (2/24) with overexpression of *MET* had also concomitant reduced or absent expression of $p16^{INK4A}$ and/or $p14^{ARF}$; 1 was an ERMS and the other was an ARMS.

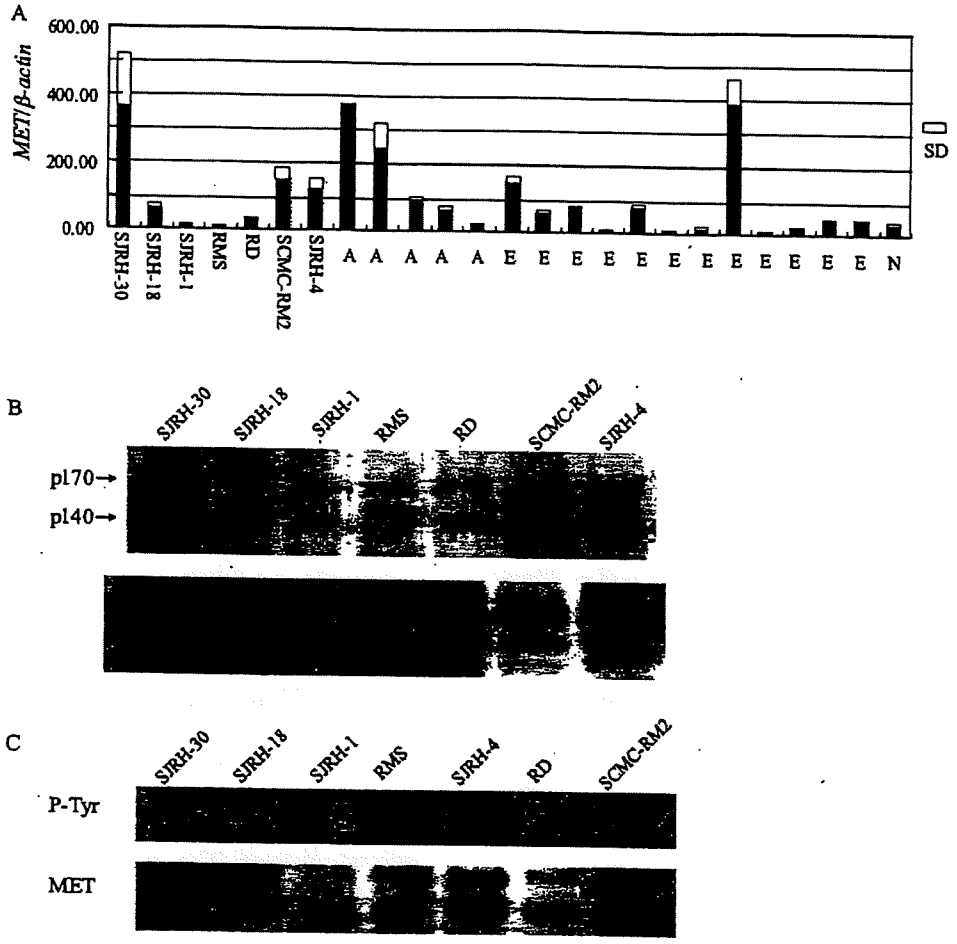

Figure 1. Expression of MET mRNA and protein in RMS. (A) Expression of *MET* mRNA (*MET*/β-*actin*) in RMS cell lines and fresh tumors as well as normal skeletal muscles detected by real-time quantitative RT-PCR. A, alveolar; E, embryonal; N, normal skeletal muscle; SD, SD. (B) Western blotting for MET in seven RMS cell lines. The arrows indicate the 170 kDa precursor and 140 kDa β-subunit, respectively. In the bottom panel, the loading of protein was shown by protein staining with Coomassie brilliant blue. (C) Tyrosine phosphorylation of MET in RMS cell lines detected by immunoprecipitation. As a control, the membrane was stripped and re-probed with anti-MET antibody, which was shown in the bottom panel.

Expression and Activation of MET Protein in RMS Cell Lines

To determine whether the expression of MET protein correlates with that of *MET* mRNA, Western blot analysis was carried out for the seven RMS cell lines. As shown in Figure 1B, a higher expression of MET protein with a mass of 140 kDa as well as a mass of 170 kDa, represented the β-subunit and precursor of MET respectively (Giordano et al., 1989), was detected in SJRH-4, SJRH-18, SJRH-30, and SCMC-RM2, consistent with the higher expression level of mRNA in these cell lines. In comparison, a relatively weak expression of p140 and p170 was detected in SJRH-1, RD and RMS, which showed a lower expression level of *MET* by RQ-PCR. The density of p140 ranged from 11.78 to 166.35 and with an average of 65.17 ± 57.00 (Table 2). The mRNA expression level of *MET* in each cell line, as detected by RQ-PCR, showed a significant correlation with the density of p140 (correlation coefficient: 0.964; $P = 0.018$).

We further studied the activation status of the MET receptor in these cell lines by immunoprecipitation analysis. As shown in Figure 1C, a band of phosphorylated MET was observed in SJRH-4, SJRH-30, and SCMC-RM2, indicating the constitutive activation of MET in these cells.

Relative DNA Copy Number of *MET* and *CDKN2A* in RMS

The relative DNA copy number of *MET* (calculated as *MET/B2M*) in the seven cell lines and 17 fresh tumors ranged from 0.60 to 1.71 with an average of 0.96 ± 0.36. No samples showed more than twice the average of the relative DNA copy

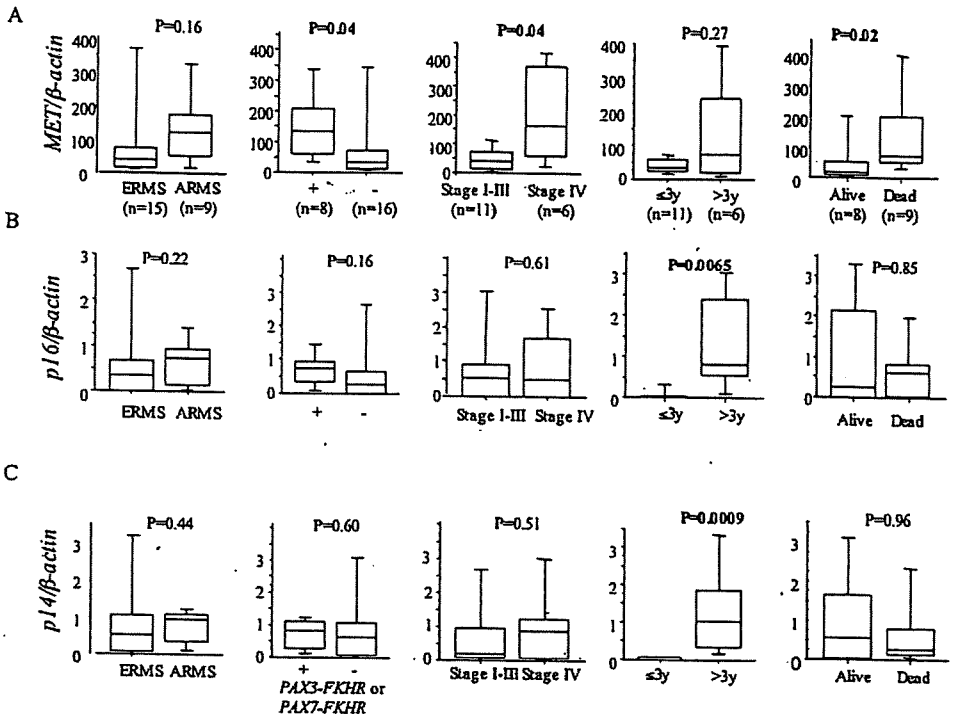

Figure 2. The relationship between clinicopathological parameters and mRNA expression of the genes *MET* (A), *p16*^{INK4A} (B), and *p14*^{ARF} (C). The expression levels of each gene were compared among groups classified by histology (including cell lines), *PAX3-FOXO1A* or *PAX7-FOXO1A* transcript expression (including cell lines), stage, age at diagnosis, as well as outcome using Mann-Whitney *U* test. It was shown in bold when $P < 0.05$.

number detected in normal skeletal muscle (1.14) or in normal PB (1.22).

The relative DNA copy number of *CDKN2A* (calculated as *CDKN2A/B2M*) was also evaluated in the 24 samples. The mean value of *CDKN2A/B2M* was 0.73 ± 0.43 with a range from 0.24 to 1.44. Three cell lines (SJRH-4, RD, RMS) (3/7) and two fresh tumors (2/17) showed less than half the mean value of the relative DNA copy number.

Expression of *PAX3-FOXO1A* and *PAX7-FOXO1A* Chimeric Transcripts in RMS

The *PAX3-FOXO1A* chimeric transcript was detected in 4 of 4 alveolar type cell lines (SJRH-4, SJRH-18, SJRH-30 and SCMC-RM2) (Table 2). There were five ARMSs among the 17 fresh tumors; 3 having *PAX3-FOXO1A* and 1 having *PAX7-FOXO1A* (4/5). Of the 4 alveolar type cell lines with expression of *PAX3-FOXO1A*, 3 showed overexpression of *MET* and of the 3 ARMSs having *PAX3-FOXO1A*, 2 showed overexpression of *MET*. The sample having *PAX7-FOXO1A* showed an expression level of *MET*/β-*actin* at 21.37 ± 1.04.

Mutations of *TP53* in RMS

The mutations of *TP53* were detected in 5/7 cell lines and 3/17 fresh tumors. The mutations in five cell lines included four missense mutations (Gly187Cys, Tyr205Cys, Tyr220Cys, and Arg248Trp) and a 13 bp deletion (nucleotides 701–713) in exon 5, which resulted in a truncated transcript (Table 2). In the five cell lines having mutations of *TP53*, two showed overexpression of *MET*. The three fresh tumors having mutations of *TP53* included an insertion of 6 bp (ACTACA) between nucleotides 960 and 961 in an ERMS (GenBank accession number: NM_000546), a missense mutation (Asp49His) in an ERMS, and a nonsense mutation (Arg → stop codon) at codon 342 in the ARMS with *PAX7-FOXO1A*. Overexpression of *MET* was only detected in one of the three samples having mutations of *TP53*.

Relationship Between the Expression Level of *MET* or *p16*^{INK4A}/*p14*^{ARF} and Clinicopathological Parameters in RMS

To address the relationship between the clinicopathological parameters and the expression levels of *MET* and *p16*^{INK4A}/*p14*^{ARF}, we compared the expression level of each gene between groups classified by patients' age, stage, histology, *PAX3-FOXO1A* or *PAX7-FOXO1A* transcript expression, as well as outcome (Fig. 2). By nonparametric

Mann-Whitney *U* test, we found that the patients with stage IV showed higher expression of *MET* than those with stage I–III ($P = 0.04$). Furthermore, the expression level of *MET* was significantly higher in the patients who died of cancer than those who were alive ($P = 0.02$). In all samples including cell lines, the group with *PAX3-FOXO1A* or *PAX7-FOXO1A* transcript showed higher expression of *MET* than that without such transcripts ($P = 0.04$). There was no statistical significance between the groups classified by histology ($P = 0.16$) and age ($P = 0.27$), although a tendency of higher expression of *MET* was shown in ARMS as well as in patients over 3 years old (Fig. 2A). Using the median expression level (58.30) as a cutoff, we also compared the difference in proportions among groups by Fisher's exact test. In all samples, overexpression of *MET* (>58.30) was detected in 7 of 9 ARMSs compared with that in 5 of 15 ERMSs ($P = 0.05$), as well as in 7 of 8 samples with *PAX3-FOXO1A* or *PAX7-FOXO1A* transcripts compared with that in 5 of 16 samples without such transcripts ($P = 0.03$). In fresh tumors, overexpression of *MET* was shown in 7 of 9 patients who died of cancer but only in 1 of 8 patients who survived ($P = 0.03$), as well as in 5 of 6 patients with stage IV compared with 3 of 11 patients with stage I–III ($P = 0.05$). The survival curve on Kaplan-Meier analyses showed that higher expression of *MET* correlated with poorer survival ($P = 0.05$, log-rank test) (Fig. 3).

On the other hand, significantly lower expression levels of $p16^{INK4A}$ and $p14^{ARF}$ were found in patients younger than 3 years ($P = 0.0065$ and $P = 0.0009$, respectively); however, the expression levels of $p16^{INK4A}$ and $p14^{ARF}$ showed no significant difference between groups classified by stage, histology, expression of *PAX3-FOXO1A* or *PAX7-FOXO1A* transcript, or prognosis (Mann-Whitney *U* test; Figs. 2B and 2C).

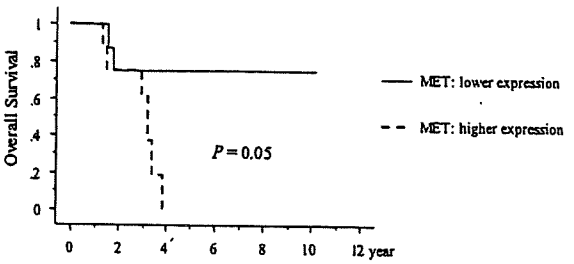

Figure 3. Kaplan-Meier curve for overall survival rates of patients with higher (>median) or lower expression (≤median) of *MET*. *P* value was calculated by log-rank test.

DISCUSSION

It has been reported that HGF/SF-MET signals induce proliferative and antiapoptotic responses in various cell types (Trusolino and Comoglio, 2002; Birchmeier et al., 2003). Analyses of HGF/SF and Met in mice have shown their essential regulatory role in development, such as the growth and survival of epithelial cells and migration of myogenic precursor cells (Bladt et al., 1995; Schmidt et al., 1995; Uehara et al., 1995). Upregulation of MET and HGF/SF expression is observed in several injured tissues, whereas deregulation of MET and HGF/SF signaling has emerged as a crucial feature of many human malignancies. For instance, germline or somatic activating mutations in the tyrosine kinase domain of *MET* have been demonstrated in papillary renal carcinomas (Schmidt et al., 1997), in childhood hepatocellular cancer (Park et al., 1999), and in metastases of carcinoma (Lorenzato et al., 2002). Overexpression and/or amplification of *MET* with autocrine or paracrine loop have been noted in carcinomas of breast (Tuck et al., 1996), thyroid (Di Renzo et al., 1992), and pancreas (Di Renzo et al., 1995), as well as in sarcomas, such as osteosarcoma (Ferracini et al., 1995) and RMS (Ferracini et al., 1996). Characterization of MET and HGF/SF activities in proliferation, invasion, angiogenesis, and antiapoptosis delineates the stages at which these molecules participate in tumor progression (Birchmeier et al., 2003). Furthermore, a number of studies have shown that HGF/SF and/or MET over- or misexpression often correlates with poor prognosis in many malignancies (Birchmeier et al., 2003). It is also reported that Pax3 modulates the expression of *Met* during limb muscle development by mediating the migration of myogenic precursor cells into the limb anlage (Bladt et al., 1995; Epstein et al., 1996), while the expression of *MET* is repressed in differentiated myotubes and in adult nondividing muscle cells (Sonnenberg et al., 1993). The *PAX3-FOXO1A* fusion protein upregulates the expression of *MET* in alveolar type RMS (Ginsberg et al., 1998).

In this study, we detected the expression of *MET* in all of the RMS samples by RQ-PCR and the expression levels showed a large variety among samples. This is comparable to an early report that the expression of *MET* was detected in 6 of 6 RMS cell lines and 9 of 14 RMS fresh tumors by Western blot analysis (Ferracini et al., 1996). In their study, cell lines RD and SJRH-30 with a higher expression of MET also showed amplification of *MET* on Southern blot analysis, whereas SJRH-1 and SJRH-4 with a relatively lower expression level showed no amplification. We found that the expression level of

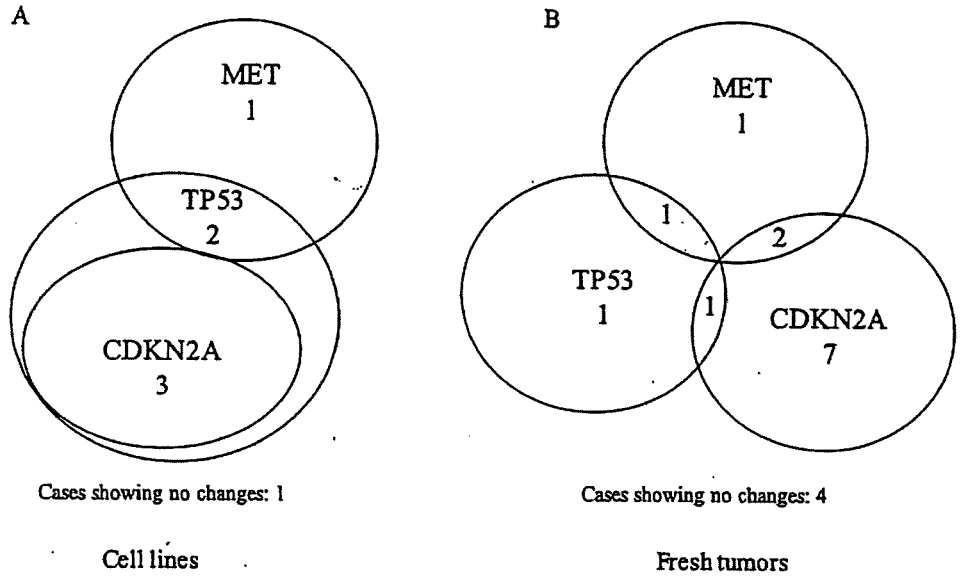

Figure 4. The distributions of overexpression of *MET* (> mean value), reduced or absent expression of $p16^{INK4A}$ and $p14^{ARF}$ (< half the mean value), and the mutations of *TP53* in seven cell lines (A) and 17 fresh tumors (B).

MET is higher in ARMS cell lines SJRH-4, SJRH-18, SCMC-RM2, and SJRH-30 than in ERMS cell lines SJRH-1, RMS, and RD by RQ-PCR (Fig. 1A). These results were also consistent with the results of Western blotting for MET protein expression. Furthermore, immunoprecipitation analysis showed constitutive tyrosine phosphorylation of MET in SJRH-4, SJRH-30, and SCMC-RM2, which indicated an autocrine manner. There was no obvious change of the relative DNA copy number observed by RQ-PCR and no mutations detected by PCR-SSCP in all samples. Thus, our results indicated that overexpression of *MET* in RMS was probably not induced by amplification/hyperploidy and that mutations of *MET* may not be of major pathogenetic importance in RMS.

Our data also showed a significantly higher expression level of *MET* in patients who died of cancer than in patients who were alive. The higher expression level was also observed in patients with stage IV as well as in patients with chimeric transcripts. A tendency toward higher *MET* expression was observed in ARMS as well as in patients over 3 years of age. Similar results were obtained when using the median level as a cutoff for *MET* expression. The survival curve on Kaplan-Meier analyses further confirmed that the expression level of *MET* correlates with the outcome of RMS patients. In RMS, it has previously been shown that older age at diagnosis, advanced stage, alveolar type, and expression of *PAX3-FOXO1A* are associated with poor prognosis (Crist et al., 1990; Newton et al., 1995; Sorensen et al., 2002). Earlier studies have also suggested that HGF/SF stimulates transmigration and invasiveness of RMS cells in vitro (Ferracini et al., 1996). It has also been reported recently that Met is necessary for a *Pax3-Foxo1a*-mediated effect in mice, and that Met has a role in RMS maintenance (Taulli et al., 2006). Taken together, it seems that MET may play an important role in the progression of RMS. A larger panel of samples should be studied to confirm this.

The *CDKN2A* gene encodes two unrelated proteins that function in tumor suppression. $p16^{INK4A}$ binds to and inhibits the activity of CDK4 and CDK6, and $p14^{ARF}$ promotes MDM2 (transformed 3T3 cell double min 2, TP53 binding protein) degradation and arrests the cell cycle in a TP53-dependent manner (Zhang et al., 1998). Thus, deletion of the *CDKN2A* locus simultaneously impairs both INK4A-cyclinD/CDK4-RB and ARF-MDM2-TP53 pathways. Mutations, homozygous deletions and altered expression of *CDKN2A* have been discovered in a wide range of human solid tumors as well as hematological malignancies (Kamb et al., 1994; Okamoto et al., 1994; Ohnishi et al., 1995; Takita et al., 2004). There has been some controversy about the significance of $p16^{INK4A}/p14^{ARF}$ in predicting the prognosis of malignancies such as neuroblastoma (Takita et al., 1998; Omura-Minamisawa et al., 2001) and childhood acute lymphoblastic leukemia (Mekki et al., 1999; Dalle et al., 2002). The association of $p16^{INK4A}$ and $p14^{ARF}$ expression with prognosis in RMS has not been well docu-

mented. In this study, we identified a nonsense mutation at codon 80 of $p16^{INK4A}$ in one cell line, SJRH-18, resulting in reduced expression of both $p16^{INK4A}$ and $p14^{ARF}$. This result is consistent with an early report showing that *CDKN2A* mutations are rare in RMS (Iolascon et al., 1996). No significant correlation was shown between the reduced or absent expression of $p16^{INK4A}$ and $p14^{ARF}$ and the clinicopathological factors, except for patients' age, which showed that the expression levels of $p16^{INK4A}$ and $p14^{ARF}$ were significantly lower in patients younger than 3 years. There were 3 of 7 cell lines (two ERMSs and one ARMS) and 2 of 17 fresh tumors (one ERMS and one ARMS) having less than a half of the mean DNA copy number, which suggested a loss of heterozygosity (LOH) in these samples; however, no homozygous deletion of *CDKN2A* was detected. The mRNA expression level of $p16^{INK4A}$ and $p14^{ARF}$ showed no obvious correlation with the relative DNA copy number.

Marked synergism between aberrant Met signaling and *Ink4a/Arf* inactivation has been shown to induce RMS at high frequency in mice (Sharp et al., 2002). Furthermore, *Pax3-Foxo1a* homozygosity with accompanying Ink4a/Arf or Tp53 pathway disruption substantially increases the frequency of alveolar RMS tumor formation in mice (Keller et al., 2004a). As shown in Figure 4A, 2 cell lines with overexpression of *MET* also had mutations of *TP53*; however, no cell lines with overexpression of *MET* showed reduced or absent expression of *CDKN2A*. Interestingly, all of the cell lines with reduced or absent expression of *CDKN2A* had mutations of *TP53*. Of 17 fresh tumors (Fig. 4B), 10 showed reduced or absent expression of *CDKN2A*; 2 of them with overexpression of *MET* and 1 of them having mutation of *TP53* simultaneously. One sample with overexpression of *MET* had mutation of *TP53*. Only 1 of 7 cell lines and 1 of 17 fresh tumors showed overexpression of *MET* alone, and one cell line and four fresh tumors did not show changes in any of the three genes.

In conclusion, our data suggest that *MET*, *CDKN2A* as well as *TP53* are involved in the pathogenesis of RMS, and that *MET* may play an important role in the progression of RMS. Molecules that specifically inhibit MET and HGF/SF are therefore promising in the treatment of RMS patients predicted to have poor prognosis.

ACKNOWLEDGMENTS

We thank Mrs. S. Soma, Miss E. Matsui, and Mrs. H. Soga for their excellent technical assistance.

REFERENCES

Birchmeier C, Birchmeier W, Gherardi E, Vande Woude GF. 2003. Met, metastasis, motility and more. Nat Rev Mol Cell Biol 4:915–925.

Bladt F, Riethmacher D, Isenmann S, Aguzzi A, Birchmeier C. 1995. Essential role for the c-met receptor in the migration of myogenic precursor cells into the limb bud. Nature 376:768–771.

Buckingham M, Bajard L, Chang T, Daubas P, Hadchouel J, Meilhac S, Montarras D, Rocancourt D, Relaix F. 2003. The formation of skeletal muscle: From somite to limb. J Anat 202:59–68.

Chen Y, Takita J, Hiwatari M, Igarashi T, Hanada R, Kikuchi A, Hongo T, Taki T, Ogasawara M, Shimada A, Hayashi Y. 2006. Mutations of the PTPN11 and RAS genes in rhabdomyosarcoma and pediatric hematological malignancies. Genes Chromosomes Cancer 45:583–591.

Chen YY, Takita J, Chen YZ, Yang HW, Hanada R, Yamamoto K, Hayashi Y. 2003. Genomic structure and mutational analysis of the human KIF1Bα gene located at 1p36.2 in neuroblastoma. Int J Oncol 23:737–744.

Chen YY, Takita J, Tanaka K, Ida K, Koh K, Igarashi T, Hanada R, Kikuchi A, Tanaka Y, Toyoda Y, Hayashi Y. 2005. Aberrations of the CHK2 gene are rare in pediatric solid tumors. Int J Mol Med 16:85–91.

Crist WM, Garnsey L, Beltangady MS, Gehan E, Ruymann F, Webber B, Hays DM, Wharam M, Maurer HM, Intergroup Rhabdomyosarcoma Committee. 1990. Prognosis in children with rhabdomyosarcoma: A report of the intergroup rhabdomyosarcoma studies I and II. J Clin Oncol 8:443–452.

Dagher R, Helman L. 1999. Rhabdomyosarcoma: An overview. Oncologist 4:34–44.

Dalle JH, Fournier M, Nelken B, Mazingue F, Lai JL, Bauters F, Fenaux P, Quesnel B. 2002. p16(INK4a) immunocytochemical analysis is an independent prognostic factor in childhood acute lymphoblastic leukemia. Blood 99:2620–2623.

Davis RJ, D'Cruz CM, Lovell MA, Biegel JA, Barr FG. 1994. Fusion of PAX7 to FKHR by the variant t(1;13)(p36;q14) translocation in alveolar rhabdomyosarcoma. Cancer Res 54:2869–2872.

Di Renzo MF, Olivero M, Ferro S, Prat M, Bongarzone I, Pilotti S, Belfiore A, Costantino A, Vigneri R, Pierotti MA, Comoglio PM. 1992. Overexpression of the c-MET/HGF receptor gene in human thyroid carcinomas. Oncogene 7:2549–2553.

Di Renzo MF, Poulsom R, Olivero M, Comoglio PM, Lemoine NR. 1995. Expression of the Met/hepatocyte growth factor receptor in human pancreatic cancer. Cancer Res 55:1129–1138.

Epstein JA, Shapiro DN, Cheng J, Lam PY, Maas RL. 1996. Pax3 modulates expression of the c-Met receptor during limb muscle development. Proc Natl Acad Sci USA 93:4213–4218.

Ferracini R, Di Renzo MF, Scotlandi K, Baldini N, Olivero M, Lollini P, Cremona O, Campanacci M, Comoglio PM. 1995. The Met/HGF receptor is over-expressed in human osteosarcomas and is activated by either a paracrine or an autocrine circuit. Oncogene 10:739–749.

Ferracini R, Olivero M, Di Renzo MF, Martano M, De Giovanni C, Nanni P, Basso G, Scotlandi K, Lollini PL, Comoglio PM. 1996. Retrogenic expression of the MET proto-oncogene correlates with the invasive phenotype of human rhabdomyosarcomas. Oncogene 12:1697–1705.

Galili N, Davis RJ, Fredericks WJ, Mukhopadhyay S, Rauscher FJ, III, Emanuel BS, Rovera G, Barr FG. 1993. Fusion of a fork head domain gene to PAX3 in the solid tumour alveolar rhabdomyosarcoma. Nat Genet 5:230–235.

Ginsberg JP, Davis RJ, Bennicelli JL, Nauta LE, Barr FG. 1998. Up-regulation of MET but not neural cell adhesion molecule expression by the PAX3-FKHR fusion protein in alveolar rhabdomyosarcoma. Cancer Res 58:3542–3546.

Giordano S, Di Renzo MF, Narsimhan RP, Cooper CS, Rosa C, Comoglio PM. 1989. Biosynthesis of the protein encoded by the c-met proto-oncogene. Oncogene 4:1383–1388.

Iolascon A, Faienza MF, Coppola B, Rosolen A, Basso G, Della Ragione F, Schettini F. 1996. Analysis of cyclin-dependent kinase inhibitor genes (CDKN2A, CDKN2B, and CDKN2C) in childhood rhabdomyosarcoma. Genes Chromosomes Cancer 15:217–222.

Jeffers M, Rong S, Woude GF. 1996. Hepatocyte growth factor/scatter factor-Met signaling in tumorigenicity and invasion/metastasis. J Mol Med 74:505–513.

Kamb A, Gruis NA, Weaver-Feldhaus J, Liu Q, Harshman K, Tavtigian SV, Stockert E, Day RS, III, Johnson BE, Skolnick MH. 1994. A cell cycle regulator potentially involved in genesis of many tumor types. Science 264:436–440.

Keller C, Arenkiel BR, Coffin CM, El-Bardeesy N, DePinho RA, Capecchi MR. 2004a. Alveolar rhabdomyosarcomas in conditional

Pax3: Fkhr mice: Cooperativity of Ink4a/ARF and Trp53 loss of function. Genes Dev 18:2614–2626.
Keller C, Hansen MS, Coffin CM, Capecchi MR. 2004b. Pax3: Fkhr interferes with embryonic Pax3 and Pax7 function: Implications for alveolar rhabdomyosarcoma cell of origin. Genes Dev 18: 2608–2613.
Lagutina I, Conway SJ, Sublett J, Grosveld GC. 2002. Pax3-FKHR knock-in mice show developmental aberrations but do not develop tumors. Mol Cell Biol 22:7204–7216.
Lillington DM, Goff LK, Kingston JE, Onadim Z, Price E, Domizio P, Young BD. 2002. High level amplification of N-MYC is not associated with adverse histology or outcome in primary retinoblastoma tumours. Br J Cancer 87:779–782.
Lorenzato A, Olivero M, Patane S, Rosso E, Oliaro A, Comoglio PM, Di Renzo MF. 2002. Novel somatic mutations of the MET oncogene in human carcinoma metastases activating cell motility and invasion. Cancer Res 62:7025–7030.
Matsumoto K, Nakamura T. 1996. Emerging multipotent aspects of hepatocyte growth factor. J Biochem (Tokyo) 119:591–600.
Mekki Y, Catallo R, Bertrand Y, Manel AM, Ffrench P, Baghdassarian N, Duhaut P, Bryon PA, Ffrench M. 1999. Enhanced expression of p16ink4a is associated with a poor prognosis in childhood acute lymphoblastic leukemia. Leukemia 13:181–189.
Merlino G, Helman LJ. 1999. Rhabdomyosarcoma—working out the pathways. Oncogene 18:5340–5348.
Newton WA, Jr., Gehan EA, Webber BL, Marsden HB, van Unnik AJ, Hamoudi AB, Tsokos MG, Shimada H, Harms D, Schmidt D, Ninfo V, Cavazzana AO, Gonzalez-Crussi F, Parham DM, Reiman HM, Asmar L, Beltangady MS, Sachs NE, Triche TJ, Maurer HM. 1995. Classification of rhabdomyosarcomas and related sarcomas. Pathologic aspects and proposal for a new classification—An Intergroup Rhabdomyosarcoma study. Cancer 76:1073–1085.
Ohnishi H, Kawamura M, Ida K, Sheng XM, Hanada R, Nobori T, Yamamori S, Hayashi Y. 1995. Homozygous deletions of p16/MTS1 gene are frequent but mutations are infrequent in childhood T-cell acute lymphoblastic leukemia. Blood 86:1269–1275.
Okamoto A, Demetrick DJ, Spillare EA, Hagiwara K, Hussain SP, Bennett WP, Forrester K, Gerwin B, Serrano M, Beach DH, Harris CC. 1994. Mutations and altered expression of p16INK4 in human cancer. Proc Natl Acad Sci USA 91:11045–11049.
Omura-Minamisawa M, Diccianni MB, Chang RC, Batova A, Bridgeman LJ, Schiff J, Cohn SL, London WB, Yu AL. 2001. p16/p14(ARF) cell cycle regulatory pathways in primary neuroblastoma: p16 expression is associated with advanced stage disease. Clin Cancer Res 7:3481–3490.
Orlow I, Roy P, Barz A, Canchola R, Song Y, Berwick M. 2001. Validation of denaturing high performance liquid chromatography as a rapid detection method for the identification of human INK4A gene mutations. J Mol Diagn 3:158–163.
Park WS, Dong SM, Kim SY, Na EY, Shin MS, Pi JH, Kim BJ, Bae JH, Hong YK, Lee KS, Lee SH, Yoo NJ, Jang JJ, Pack S, Zhuang Z, Schmidt L, Zbar B, Lee JY. 1999. Somatic mutations in the kinase domain of the Met/hepatocyte growth factor receptor gene in childhood hepatocellular carcinomas. Cancer Res 59:307–310.
Robertson KD, Jones PA. 1999. Tissue-specific alternative splicing in the human INK4a/ARF cell cycle regulatory locus. Oncogene 18:3810–3820.
Schmidt C, Bladt F, Goedecke S, Brinkmann V, Zschiesche W, Sharpe M, Gherardi E, Birchmeier C. 1995. Scatter factor/hepatocyte growth factor is essential for liver development. Nature 373:699–702.
Schmidt L, Duh FM, Chen F, Kishida T, Glenn G, Choyke P, Scherer SW, Zhuang Z, Lubensky I, Dean M, Allikmets R, Chidambaram A, Bergerheim UR, Feltis JT, Casadevall C, Zamarron A, Bernues M, Richard S, Lips CJ, Walther MM, Tsui LC, Geil L, Orcutt ML, Stackhouse T, Lipan J, Slife L, Brauch H, Decker J, Niehans G, Hughson MD, Moch H, Storkel S, Lerman MI, Linehan WM, Zbar B. 1997. Germline and somatic mutations in the tyrosine kinase domain of the MET proto-oncogene in papillary renal carcinomas. Nat Genet 16:68–73.
Sharp R, Recio JA, Jhappan C, Otsuka T, Liu S, Yu Y, Liu W, Anver M, Navid F, Helman LJ, DePinho RA, Merlino G. 2002. Synergism between INK4a/ARF inactivation and aberrant HGF/SF signaling in rhabdomyosarcomagenesis. Nat Med 8:1276–1280.
Sherr CJ. 2001. The INK4a/ARF network in tumour suppression. Nat Rev Mol Cell Biol 2:731–737.
Shibuya N, Taki T, Mugishima H, Chin M, Tsuchida M, Sako M, Kawa K, Ishii E, Miura I, Yanagisawa M, Hayashi Y. 2001. t(10;11)-acute leukemias with MLL-AF10 and MLL-ABI1 chimeric transcripts: Specific expression patterns of ABI1 gene in leukemia and solid tumor cell lines. Genes Chromosomes Cancer 32:1–10.
Skapek SX, Rhee J, Spicer DB, Lassar AB. 1995. Inhibition of myogenic differentiation in proliferating myoblasts by cyclin D1-dependent kinase. Science 267:1022–1024.
Sonnenberg E, Meyer D, Weidner KM, Birchmeier C. 1993. Scatter factor/hepatocyte growth factor and its receptor, the c-met tyrosine kinase, can mediate a signal exchange between mesenchyme and epithelia during mouse development. J Cell Biol 123:223–235.
Sorensen PH, Lynch JC, Qualman SJ, Tirabosco R, Lim JF, Maurer HM, Bridge JA, Crist WM, Triche TJ, Barr FG. 2002. PAX3-FKHR and PAX7-FKHR gene fusions are prognostic indicators in alveolar rhabdomyosarcoma: A report from the children's oncology group. J Clin Oncol 20:2672–2679.
Takeo S, Arai H, Kusano N, Harada T, Furuya T, Kawauchi S, Oga A, Hirano T, Yoshida T, Okita K, Sasaki K. 2001. Examination of oncogene amplification by genomic DNA microarray in hepatocellular carcinomas: Comparison with comparative genomic hybridization analysis. Cancer Genet Cytogenet 130:127–132.
Takita J, Hayashi Y, Kohno T, Yamaguchi N, Hanada R, Yamamoto K, Yokota J. 1997. Deletion map of chromosome 9 and p16 (CDKN2A) gene alterations in neuroblastoma. Cancer Res 57:907–912.
Takita J, Hayashi Y, Nakajima T, Adachi J, Tanaka T, Yamaguchi N, Ogawa Y, Hanada R, Yamamoto K, Yokota J. 1998. The p16 (CDKN2A) gene is involved in the growth of neuroblastoma cells and its expression is associated with prognosis of neuroblastoma patients. Oncogene 17:3137–3143.
Takita J, Ishii M, Tsutsumi S, Tanaka Y, Kato K, Toyoda Y, Hanada R, Yamamoto K, Hayashi Y, Aburatani H. 2004. Gene expression profiling and identification of novel prognostic marker genes in neuroblastoma. Genes Chromosomes Cancer 40:120–132.
Taulli R, Scuoppo C, Bersani F, Accornero P, Forni PE, Miretti S, Grinza A, Allegra P, Schmitt-Ney M, Crepaldi T, Ponzetto C. 2006. Validation of met as a therapeutic target in alveolar and embryonal rhabdomyosarcoma. Cancer Res 66:4742–4749.
Trusolino L, Comoglio PM. 2002. Scatter-factor and semaphorin receptors: Cell signalling for invasive growth. Nat Rev Cancer 2:289–300.
Tuck AB, Park M, Sterns EE, Boag A, Elliott BE. 1996. Coexpression of hepatocyte growth factor and receptor (Met) in human breast carcinoma. Am J Pathol 148:225–232.
Uehara Y, Minowa O, Mori C, Shiota K, Kuno J, Noda T, Kitamura N. 1995. Placental defect and embryonic lethality in mice lacking hepatocyte growth factor/scatter factor. Nature 373:702–705.
Uno K, Takita J, Yokomori K, Tanaka Y, Ohta S, Shimada H, Gilles FH, Sugita K, Abe S, Sako M, Hashizume K, Hayashi Y. 2002. Aberrations of the hSNF5/INI1 gene are restricted to malignant rhabdoid tumors or atypical teratoid/rhabdoid tumors in pediatric solid tumors. Genes Chromosomes Cancer 34:33–41.
Zhang Y, Xiong Y, Yarbrough WG. 1998. ARF promotes MDM2 degradation and stabilizes p53: ARF-INK4a locus deletion impairs both the Rb and p53 tumor suppression pathways. Cell 92:725–734.

International Journal of
HEMATOLOGY

Letter to the Editor

Low Frequency of *KIT* Gene Mutation in Pediatric Acute Myeloid Leukemia with inv(16)(p13q22): A Study of the Japanese Childhood AML Cooperative Study Group

Akira Shimada,[a] Hitoshi Ichikawa,[b] Tomohiko Taki,[c] Chisato Kubota,[a] Teruaki Hongo,[d] Masahiro Sako,[e] Akira Morimoto,[f] Akio Tawa,[g] Ichiro Tsukimoto,[h] Yasuhide Hayashi[a]

[a]*Department of Hematology/Oncology, Gunma Children's Medical Center, Gunma, Japan;* [b]*Cancer Transcriptome Project, National Cancer Center Research Institute, Tokyo, Japan;* [c]*Department of Molecular Laboratory Medicine, Kyoto Prefectural University of Medicine Graduate School of Medical Science, Kyoto, Japan;* [d]*Department of Pediatrics, Hamamatsu University School of Medicine, Shizuoka, Japan;* [e]*Department of Pediatric Hematology/Oncology, Osaka City General Hospital, Osaka, Japan;* [f]*Department of Pediatrics, Kyoto Prefectural University of Medicine Graduate School of Medical Science, Kyoto, Japan;* [g]*Department of Pediatrics, National Hospital Organization Osaka National Hospital, Osaka, Japan;* [h]*First Department of Pediatrics, Toho University School of Medicine, Tokyo, Japan*

Received June 6, 2007; received in revised form June 21, 2007; accepted June 28, 2007

Int J Hematol. 2007;86:289-290. doi: 10.1532/IJH97.07098

Acute myeloid leukemia (AML) patients with t(8;21)(q22;q22) or inv(16)(p13q22) are known to have a good prognosis. Recently, mutations of the *KIT* gene have been found in 12.7% to 48.1% of adult AML patients with t(8;21) or inv(16) and in approximately 20% of pediatric AML patients with t(8;21) [1-5]. *KIT* gene mutations in adult and pediatric AML patients with t(8;21) and in adult AML patients with inv(16) have been associated with a poorer prognosis than in those without *KIT* gene mutations [1-5]. However, the frequency and clinical impact of *KIT* gene mutations in pediatric AML patients with inv(16) remain unknown. Pediatric AML patients with inv(16) have been reported to represent 3.4% to 6% of the total number of pediatric AML patients. Thus, the number of patients in this subgroup is very small [6,7].

Three hundred eighteen patients were enrolled in the Japanese Childhood AML Cooperative Study Group Protocol AML 99 from January 2000 to December 2002, and 12 (3.8%) of these AML patients comprised 11 patients with inv(16) and 1 patient with t(16;16)(p13;q22) [5,8]. The 5-year overall survival rate was 100%, and the event-free survival rate was 90.9%. Of these 12 AML patients with inv(16) or t(16;16), 7 patients were available for molecular analysis (age range, 11 months to 14 years; median, 10 years) (Table 1). The 5-year overall survival rate for these 7 patients was 100%, and the event-free survival rate was 85.7% (Table 1). We used the reverse transcriptase–polymerase chain reaction method in a mutational analysis of the extracellular domain (exons 8 and 9), the transmembrane domain (exon 10), the juxtamembrane domain (exon 11), and the second intracellular kinase domain (exons 17 and 18) of the *KIT* gene and then carried out a sequencing analysis [5]. Sequencing was performed directly or, if necessary, after subcloning.

KIT mutation (deletion of D419 in exon 8) was found in an 11-month-old male patient (1 [14.3%] of 7 patients). The initial white blood cell count for this patient (no. 7) was 199,000/μL, and a karyotype analysis revealed 46,XY,inv(16)(p13q22). This patient received a total of 6 consecutive chemotherapies; however, he relapsed 16 months after the initial diagnosis. He then underwent unrelated allogeneic stem cell transplantation during the second complete remission and has been alive for 40 months from the diagnosis. The remaining 6 AML patients with inv(16) have maintained a complete remission without relapse for more than 41 months.

As for *FLT3* and *RAS* gene alterations, we found 2 *FLT3* D835 mutations (28.6%) and 2 *NRAS* mutations (28.6%) in these 7 AML patients with inv(16) (Table 1). No patient had an *FLT3* internal tandem duplication or a *KRAS* gene mutation. The majority of these patients (5 [71.4%] of 7) had one of the chimeric *CBFβ-MYH11* transcripts, which have most frequently been found in AML cases with inv(16) (*CBFβ* at nucleotide 495 fused to

Correspondence and reprint requests: Yasuhide Hayashi, MD, Director, Gunma Children's Medical Center, 779 Shimohakoda, Hokkitsu, Shibukawa, Gunma 377-8577, Japan; 81-279-52-3551 ext 201; fax: 81-279-52-2045 (e-mail: hayashiy-tky@umin.ac.jp).

Table 1.
Correlations of Clinical Features with *KIT*, *FLT3*, and *RAS* Gene Mutations in 7 Acute Myeloid Leukemia Patients with inv(16) or t(16;16)*

Patient No.	Age	Sex	FAB Classification	Karyotype	*CBFβ-MYH11*	*KIT* Mt	*FLT3* D835 Mt	*NRAS* Mt	EFS Time, mo
1	14 y	M	M4Eo	46,XY,inv(16)(p13q22), add(7)(q32)	†	–	–	+‡	63+
2	10 y	M	M4Eo	46,XY,inv(16)(p13q22)	1	–	–	–	67+
3	7 y	M	M1	46,XY,inv(16)(p13q22)	1	–	–	–	63+
4	13 y	F	M1	46,XX,inv(16)(p13q22)	1	–	+	–	59+
5	3 y	F	M5a	47,XX,+8,t(16;16)(p13;q22)	2	–	–	+‡	43+
6	14 y	F	M5b	46,XX,inv(16)(p13q22)	1	–	+	–	41+
7	11 mo	M	M4Eo	46,XY,inv(16)(p13q22)	1	+§	–	–	16

**CBFβ-MYH11* transcripts were detected by reverse transcriptase–polymerase chain reaction analysis and direct sequencing (1, nucleotide 495 of *CBFβ* fused to nucleotide 1921 of *MYH11*; 2, nucleotide 399 of *CBFβ* fused to nucleotide 1201 of *MYH11*). *KRAS* mutations were not found in any of the 7 patients. FAB, French-American-British; Mt, mutation; EFS, event-free survival.

†Chimeric transcripts were not detected.

‡Codon 12.

§Deletion D419 in exon 8.

MYH11 at nucleotide 1921, Table 1) [9,10]. The *FLT3* D835 mutation, *NRAS* mutation, and subtypes of *CBFβ-MYH11* transcripts were not associated with the clinical outcome.

We also looked for *KIT* mutations in 11 pediatric AML patients with inv(16) who were treated with the previous protocol in Japan (age range, 8 months to 15 years; median, 3 years), but we did not identify *KIT* mutations in any of the patients. Interestingly, 3 of the 11 AML patients with inv(16) were infants, and 2 of them died, although all 3 exhibited no mutations in *KIT*, *FLT3*, or *RAS*. These data together with those described in our previous report [11] suggest that infant AML patients with inv(16) have a poor prognosis, regardless of the status of these genes.

A few reports have suggested that adult AML patients who have inv(16) with *KIT* mutations were associated with a poorer prognosis than those without KIT mutations [2,3]. A recent study by the Berlin-Frankfurt-Münster Study Group revealed that 6 (54.5%) of 11 pediatric AML patients with inv(16) had *KIT* mutations but that the clinical impact was limited [12]. The Acute Leukemia French Association (ALFA) and the Leucémies Aiguës Myéloblastiques de l'Enfant (LAME) cooperative study groups also suggested that *KIT* gene mutations were not associated with a poor prognosis in pediatric and adult AML patients with inv(16) [4]. We considered the frequency of *KIT* gene mutations (1 [5.6%] of 18) among the pediatric AML patients with inv(16) in this study to be lower than that of adult AML patients with inv(16) [2-4]. We must await the results of a larger study regarding the correlation between *KIT* gene mutations and prognosis in pediatric AML patients with inv(16).

Acknowledgments

This work was supported in part by a Grant-in-Aid for Cancer Research and a Grant for Clinical Cancer Research and Research on Children and Families from the Ministry of Health, Labor and Welfare of Japan. This work was also supported by a Grant-in-Aid for Scientific Research (C) from the Ministry of Education, Culture, Sports, Science and Technology of Japan and a Research Grant for Gunma Prefectural Hospitals.

References

1. Beghini A, Peterlongo P, Ripamonti CB, et al. C-kit mutations in core binding factor leukemias. *Blood.* 2000;95:726-727.
2. Care RS, Valk PJ, Goodeve AC, et al. Incidence and prognosis of c-KIT and FLT3 mutations in core binding factor (CBF) acute myeloid leukaemias. *Br J Haematol.* 2003;121:775-777.
3. Paschka P, Marcucci G, Ruppert AS, et al. Adverse prognostic significance of KIT mutations in adult acute myeloid leukemia with inv(16) and t(8;21): a Cancer and Leukemia Group B study. *J Clin Oncol.* 2006;24:3904-3911.
4. Boissel N, Leroy H, Brethon B, et al, for the Acute Leukemia French Association (ALFA) and the Leucémies Aiguës Myéloblastiques de l'Enfant (LAME) Cooperative Groups. Incidence and prognostic impact of c-Kit, FLT3, and Ras gene mutations in core binding factor acute myeloid leukemia (CBF-AML). *Leukemia.* 2006;20:965-970.
5. Shimada A, Taki T, Tabuchi K, et al. KIT mutations, and not FLT3 internal tandem duplication, are strongly associated with a poor prognosis in pediatric acute myeloid leukemia with t(8;21): a study of the Japanese Childhood AML Cooperative Study Group. *Blood.* 2006;107:1806-1809.
6. Grimwade D, Walker H, Oliver F, et al, on behalf of the Medical Research Council Adult and Children's Leukaemia Working Parties. The importance of diagnostic cytogenetics on outcome in AML: analysis of 1,612 patients entered into the MRC AML 10 trial. *Blood.* 1998;92:2322-2333.
7. Forestier E, Heim S, Blennow E, et al. Cytogenetic abnormalities in childhood acute myeloid leukaemia: a Nordic series comprising all children enrolled in the NOPHO-93-AML trial between 1993 and 2001. *Br J Haematol.* 2003;121:566-577.
8. Kobayashi R, Tawa A, Hanada R, Horibe K, Tsuchida M, Tsukimoto I, for the Japanese childhood AML cooperative study group. Extramedullary infiltration at diagnosis and prognosis in children with acute myelogenous leukemia. *Pediatr Blood Cancer.* 2007;48:393-398.
9. Poirel H, Radford-Weiss I, Rack K, et al. Detection of the chromosome 16 CBF beta-MYH11 fusion transcript in myelomonocytic leukemias. *Blood.* 1995;85:1313-1322.
10. Reilly JT. Pathogenesis of acute myeloid leukaemia and inv(16)(p13;q22): a paradigm for understanding leukaemogenesis? *Br J Haematol.* 2005;128:18-34.
11. Xu F, Taki T, Eguchi M, et al. Tandem duplication of the FLT3 gene is infrequent in infant acute leukemia. Japan Infant Leukemia Study Group. *Leukemia.* 2000;14:945-947.
12. Goemans BF, Zwaan CM, Miller M, et al. Mutations in KIT and RAS are frequent events in pediatric core-binding factor acute myeloid leukemia. *Leukemia.* 2005;19:1536-1542.

AML1 Mutation and *FLT3*-internal Tandem Duplication in Leukemia Transformed From Myelodysplastic Syndrome

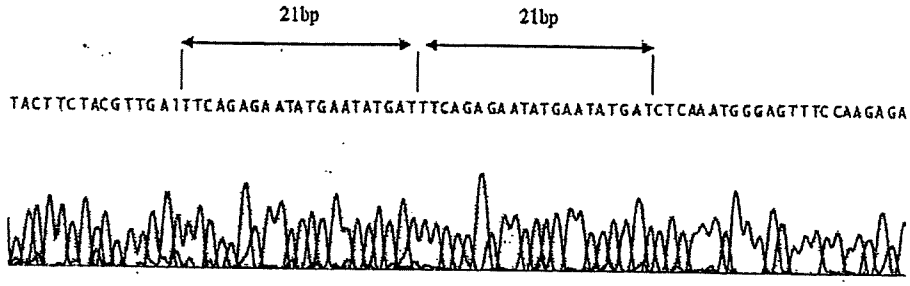

FIGURE 2. Sequence of *FLT3* gene. ITD of 21 bp in exon 11 was observed. The wild type of *FLT3* was not found.

To the Editor:

Myelodysplastic syndrome (MDS) is a clonal disorder of hematopoietic stem cells characterized by ineffective and inadequate hematopoiesis. Recently, gene alterations including *AML1/RUNX1* had been demonstrated to contribute to the development from MDS to secondary acute myeloid leukemia (AML) in adult patients, particular in AML-M0 or AML with acquired trisomy 21.[1,2] Moreover, *FLT3*-internal tandem duplication (ITD) predicts a high risk of progression of MDS to AML in adult patients,[3] but these gene alterations were rarely reported in pediatric MDS.[4]

We reported here a 6-year-old girl with leukocytosis, which consisted of monocytosis and immature myeloid cells. She did not show hepatomegaly, splenomegaly, café-au-lait spots, or other abnormal physical findings. A bone marrow aspirate showed a hypercellular marrow with greatly increased myeloid cells and megakaryocytes, but blasts were less than 1%. Only minimal dysplastic change was seen in her bone marrow cells with normal female karyotype. A provisional diagnosis was adult-type chronic myelomonocytic leukemia. She developed acute mixed-lineage leukemia carrying trisomy 21 after 4 years from the initial diagnosis. The disease progressed rapidly, and she died after allogeneic stem cell transplantation.

We analyzed mutations in the runt domain of *AML1*gene by polymerase chain reaction or reverse-transcription polymerase chain reaction followed direct sequencing using the primers previously described.[5] The patient had a mutation within intron 3 of *AML1* gene (T to A; −10 from exon 4, Fig. 1). The mutation led to an 8-bp insertion on 1 mRNA allele resulting from change in a splicing acceptor site in intron 3; this induced a frameshift that produced a stop codon. Both normal and mutant *AML1* sequences were found in this patient (Fig. 1).

Moreover, we analyzed the juxtermembrane domain of the *FLT3* gene using primer pairs R5 and R6[6] and found an ITD of 21 bp in exon 11 (Fig. 2), but we could not find the wild-type product of *FLT3* gene. Moreover, mutations of *RAS* and *PTPN11* genes were not found in this patient.

Interestingly, dual mutations in the *AML1* and *FLT3* genes were found in AML-M0 subtype in adult MDS patients.[7] We considered that both *AML1* mutation and *FLT3*-ITD may have a role in disease progression. However, we could not examine the *AML1* mutation and *FLT3*-ITD at the time of chronic phase because the sample was not available. Larger studies regarding gene alterations in pediatric MDS will be needed to clarify these associations.

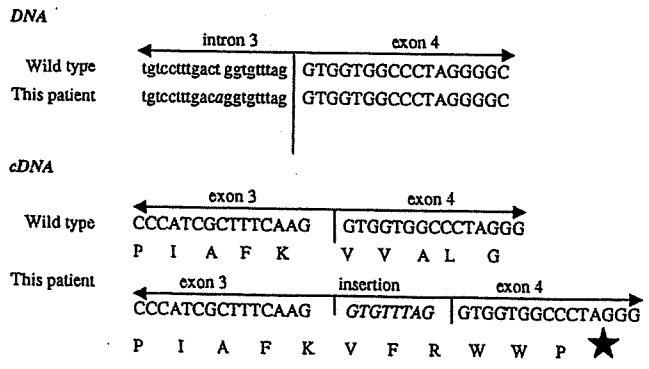

FIGURE 1. The schema of mutation in the runt domain of the *AML1/RUNX1* gene. A point mutation at intron 3 (t→a; italic letter -10 from exon 4), led to an 8-bp insertion (italic letters) on 1 cDNA allele because of the change in the splicing acceptor site in intron 3, inducing a frameshift resulting in a stop codon (pentagram). The wild type of *AML1* was also found.

Akira Shimada, MD*†
Takeshi Taketani, MD‡
Akira Kikuchi, MD†
Ryoji Hanada, MD†
Hiroshi Arakawa, MD§
Hirokazu Kimura, PhD‖
Yuyan Chen, MD¶
Yasuhide Hayashi, MD*
*Department of Hematology/Oncology
Gunma Children's Medical Center
Gunma
†Division of Hematology/Oncology
Saitama Children's Medical Center
§Department of Pediatrics
Saitama Medical Center
Saitama Medical School, Saitama
‖Department of Research Group, Gunma
Prefectural Institute of Public Health and
Environmental Sciences, Gunma

‡Department of Pediatrics
Graduate School of Medicine
University of Shimane, Shimane
¶Department of Pediatrics
Graduate School of Medicine
University of Tokyo, Tokyo, Japan

REFERENCES

1. Osato M, Asou N, Abdalla E, et al. Biallelic and heterozygous point mutations in the runt domain of the AML1/PEBP2alphaB gene associated with myeloblastic leukemias. *Blood.* 1999;93:1817–1824.
2. Preudhomme C, Warot-Loze D, Roumier C, et al. High incidence of biallelic point mutations in the runt domain of the AML1/PEBP2 alpha B gene in Mo acute myeloid leukemia and in myeloid malignancies with acquired trisomy 21. *Blood.* 2000;96:2862–2869.
3. Shih LY, Huang CF, Wang PN, et al. Acquisition of FLT3 or N-ras mutations is frequently associated with progression of myelodysplastic syndrome to acute myeloid leukemia. *Leukemia.* 2004;18: 466–475.
4. Gratias EJ, Liu YL, Meleth S, et al. Activating FLT3 mutations are rare in children with juvenile myelomonocytic leukemia. *Pediatr Blood Cancer.* 2005;44: 142–146.
5. Taketani T, Taki T, Takita J, et al. Mutation of the AML1/RUNX1 gene in a transient myeloproliferative disorder patient with Down syndrome. *Leukemia.* 2002;16:1866–1867.
6. Xu F, Taki T, Yang HW, et al. Tandem duplication of the FLT3 gene is found in acute lymphoblastic leukaemia as well as acute myeloid leukaemia but not in myelodysplastic syndrome or juvenile chronic myelogenous leukaemia in children. *Br J Haematol.* 1999;105:155–162.
7. Matsuno N, Osato M, Yamashita N, et al. Dual mutations in the AML1 and FLT3 genes are associated with leukemogenesis in acute myeloblastic leukemia of the M0 subtype. *Leukemia.* 2003;17: 2492–2499.

Routine Use of PET Scans After Completion of Therapy in Pediatric Hodgkin Disease Results in a High False Positive Rate

In Response:

Drs Mardis and Wong raise important points in response to our published report regarding the routine use of positron emission tomography (PET) scans for surveillance of disease recurrence after completion of therapy in children and adolescents with Hodgkin lymphoma.[1] Our study was designed to evaluate PET scans as they are commonly used in the patient population. Hence, our data included all PET scans, as they are used for surveillance even when PET scans were not used in the diagnostic period. Similarly, in practice, multiple physicians read PET scans and variability in interpretation is itself a limitation of the use of PET scans. Drs Mardis and Wong note that perhaps some of false positives in the early stages were due to inexperience, however, we presented information that the false positive rate remained the same throughout the study period suggesting that a learning curve did not account for the findings of the study.

Since our publication Meany et al[2] published a study, evaluating 23 consecutive pediatric patients with Hodgkin disease and compared PET scan results with clinical status and computed tomography (CT) scans. Their results included a strong negative predictive value of 100% and a positive predictive value of 18.2%, findings that are almost identical to our results. They conclude, as we did, that positive PET scans must be interpreted conservatively and that treatment decisions should not be made on the findings of a positive study.

Ultimately, Dr Mardis and Wong's conclusion that CT/PET scanners will solve many of the issues that commonly occur with the use of PET scans supports the conclusion that PET scans are not an ideal imaging modality for off therapy patients. Our concern, and the rationale for publishing our data, is that PET scans are still used in many centers where combined CT/PET scans are not available and also continue to be used in research studies. Thus, the issues that arise with the use of PET scans, including the presence of false positive results, are likely to continue to present management dilemmas to our colleagues and need to be acknowledged. The International Harmonization Project recently evaluated the existing data on the use of PET scans in lymphoma therapy.[3] Consistent with our recommendations, the report concluded that the current data is inadequate to recommend routine surveillance PET scans after completion of therapy.

Jennifer M. Levine, MSW, MD
Michael Weiner, MD
Kara M. Kelly, MD
Division of Pediatric Oncology
Columbia University Medical Center
New York, NY

REFERENCES

1. Levine JM, Weiner M, Kelly KM. Routine use of PET scans after completion of therapy in pediatric Hodgkin disease results in a high false positive rate. *J Pediatr Hematol Oncol.* 2006;28:711–714.
2. Meany HJ, Gidvani VK, Minniti CP. Utility of PET scans to predict disease relapse in pediatric patients with Hodgkin lymphoma. *Pediatr Blood Cancer.* 2007; 48:399–402.
3. Cheson BD, Pfistner B, Juweid ME, et al. Revised response criteria for malignant lymphoma. *J Clin Oncol.* 2007;25:579–586.

The Accuracy of PET(CT) in Evaluating Pediatric Lymphoma

To the Editor:

We read with great interest the recent article by Levine et al[1] in the November 2006 issue of *Journal of Pediatric Hematology/Oncology*. We have some concerns about the results of this study.

First, only a portion of the cohort had a positron emission tomography (PET) scan at initial diagnosis to serve as a reference for disease response to therapy. Correcting this deficit in surveillance might have minimized false positive results in their patient population. Besides, there was no quantification of metabolic activity, which is important in defining the underlying biologic behavior of the lymphoma. As described by Wong et al,[2] quantitative examination of the glucose metabolic rate by the

ARTICLE

Highly Sensitive Method for Genomewide Detection of Allelic Composition in Nonpaired, Primary Tumor Specimens by Use of Affymetrix Single-Nucleotide–Polymorphism Genotyping Microarrays

Go Yamamoto,* Yasuhito Nannya,* Motohiro Kato, Masashi Sanada, Ross L. Levine, Norihiko Kawamata, Akira Hangaishi, Mineo Kurokawa, Shigeru Chiba, D. Gary Gilliland, H. Phillip Koeffler, and Seishi Ogawa

Loss of heterozygosity (LOH), either with or without accompanying copy-number loss, is a cardinal feature of cancer genomes that is tightly linked to cancer development. However, detection of LOH is frequently hampered by the presence of normal cell components within tumor specimens and the limitation in availability of constitutive DNA. Here, we describe a simple but highly sensitive method for genomewide detection of allelic composition, based on the Affymetrix single-nucleotide–polymorphism genotyping microarray platform, without dependence on the availability of constitutive DNA. By sensing subtle distortions in allele-specific signals caused by allelic imbalance with the use of anonymous controls, sensitive detection of LOH is enabled with accurate determination of allele-specific copy numbers, even in the presence of up to 70%–80% normal cell contamination. The performance of the new algorithm, called "AsCNAR" (allele-specific copy-number analysis using anonymous references), was demonstrated by detecting the copy-number neutral LOH, or uniparental disomy (UPD), in a large number of acute leukemia samples. We next applied this technique to detection of UPD involving the 9p arm in myeloproliferative disorders (MPDs), which is tightly associated with a homozygous *JAK2* mutation. It revealed an unexpectedly high frequency of 9p UPD that otherwise would have been undetected and also disclosed the existence of multiple subpopulations having distinct 9p UPD within the same MPD specimen. In conclusion, AsCNAR should substantially improve our ability to dissect the complexity of cancer genomes and should contribute to our understanding of the genetic basis of human cancers.

Genomewide detection of loss of heterozygosity (LOH), as well as copy-number (CN) alterations in cancer genomes, has drawn recent attention in the field of cancer genetics,[1–3] because LOH has been closely related to the pathogenesis of cancers, in that it is a common mechanism for inactivation of tumor suppressor genes in Knudson's paradigm.[4] Moreover, the recent discovery of the activating Janus kinase 2 gene (*JAK2* [MIM *147796]) mutation that is tightly associated with the common 9p LOH with neutral CNs, or uniparental disomy (UPD), in myeloproliferative disorders (MPDs)[5–8] uncovered a new paradigm—that a dominant oncogenic mutation may be further potentiated by duplication of the mutant allele and/or exclusion of the wild-type allele—underscoring the importance of simultaneous CN detection with LOH analysis. On this point, Affymetrix GeneChip SNP-detection arrays, originally developed for large-scale SNP typing,[9] provide a powerful platform for both genomewide LOH analysis and CN detection.[10–12] On this platform, the use of large numbers of SNP-specific probes showing linear hybridization kinetics allows not only for high-resolution LOH analysis at ~2,500–150,000 heterozygous SNP loci but also for accurate determination of the CN state at each LOH region.[12–14] Unfortunately, however, the sensitivity of the currently available algorithm for LOH detection by use of SNP arrays may be greatly reduced when they are applied to primary tumor specimens that are frequently heterogeneous and contain significant normal cell components.

In this article, we describe a simple but highly sensitive method to detect allelic dosage (CNs) in primary tumor specimens on a GeneChip platform, with its validations, and some interesting applications to the analyses of primary hematological tumor samples. It does not require paired constitutive DNA of tumor specimens or a large set of normal reference samples but uses only a small number of anonymous controls for accurate determination of allele-specific CN (AsCN) even in the presence of significant

From the Departments of Hematology/Oncology (G.Y.; Y.N.; M.S.; A.H.; M. Kurokawa; S.O.), Regeneration Medicine for Hematopoiesis (S.O.), Pediatrics (M. Kato), and Cell Therapy and Transplantation Medicine (S.C.; S.O.), and The 21st Century Center of Excellence Program (Y.N.; M.S.; S.O.), Graduate School of Medicine, University of Tokyo, and Core Research for Evolutional Science and Technology, Japan Science and Technology Agency (S.O.), Tokyo; Division of Hematology, Department of Medicine, Brigham and Women's Hospital, Harvard Medical School, Boston (R.L.L.; D.G.G.); and Hematology/Oncology, Cedars-Sinai Medical Center/University of California–Los Angeles School of Medicine, Los Angeles (N.K.; H.P.K.)

Received February 2, 2007; accepted for publication April 12, 2007; electronically published June 5, 2007.

Address for correspondence and reprints: Seishi Ogawa, The 21st Century COE Program, Department of Regeneration Medicine for Hematopoiesis, Department of Cell Therapy and Transplantation Medicine, Graduate School of Medicine, University of Tokyo, 7-3-1, Hongo, Bunkyo-ku, Tokyo 113-8655, Japan. E-mail: sogawa-tky@umin.ac.jp

* These two authors contributed equally to this work.

Am. J. Hum. Genet. 2007;81:114–126. 0002-9297/2007/8101-0011$15.00
DOI: 10.1086/518809

proportions of normal cell components, thus enabling reliable genomewide detection of LOH in a wide variety of primary cancer specimens.

Material and Methods

Samples and Microarray Analysis

Genomic DNA extracted from a lung cancer cell line (NCI-H2171) was intentionally mixed with DNA from its paired lymphoblastoid cell line (LCL) (NCI-BL2171) to generate a dilution series, in which tumor contents started at 10% and increased by 10% up to 90%. The ratios of admixture were validated using measurements of a microsatellite (*D3S1279*) within a UPD region on chromosome 3 (data not shown). The nine mixed samples, together with non-mixed original DNAs (0% and 100% tumor contents), were analyzed with GeneChip 50K Xba SNP arrays (Affymetrix). Microarray data corresponding to 5%, 15%, 25%,..., and 95% tumor content were interpolated by linearly superposing two adjacent microarray data sets after adjusting the mean array signals of the two sets. Both cell lines were obtained from the American Type Culture Collection (ATCC). Genomic DNA was also extracted from 85 primary leukemia samples, including 39 acute myeloid leukemia (AML [MIM #601626]) samples and 46 acute lymphoblastic leukemia (ALL) samples, and was subjected to analysis with 50K Xba SNP arrays. Of the 85 samples, 34 were analyzed with their matched complete-remission bone marrow samples. DNA from 53 MPD samples—13 polycythemia vera (PV [MIM #263300]), 21 essential thrombocythemia (ET [MIM #187950]), and 19 idiopathic myelofibrosis (IMF [MIM #254450])—43 of which had been studied for *JAK2* mutations,[8] were also analyzed with 50K Xba SNP arrays. Microarray analyses were performed according to the manufacturer's protocol,[15] except with the use of LA *Taq* (Takara) for adaptor-mediated PCR. Also, DNA from 96 normal volunteers was used for the analysis. All clinical specimens were made anonymous and were incorporated into this study in accordance with the approval of the institutional review boards of the University of Tokyo and Harvard Medical School.

AsCN Analyses Using Anonymous Control Samples (AsCNAR)

SNP typing on the GeneChip platform uses two discrete sets of SNP-specific probes, which are arbitrarily but consistently named "type *A*" and "type *B*" SNPs, at every SNP locus, each consisting of an equal number of perfectly matched probes (PM_As or PM_Bs) and mismatched probes (MM_As or MM_Bs). For AsCN analysis, the sums of perfectly matched probes (PM_As or PM_Bs) for the *i*th SNP locus in the tumor (tum) sample and reference samples (ref1, ref2,..., ref*N*),

$$S_{A,I}^{\mathrm{tum}} = \sum \mathrm{PM}_{A,I}^{\mathrm{tum}}\ ,\quad S_{B,I}^{\mathrm{tum}} = \sum \mathrm{PM}_{B,I}^{\mathrm{tum}}$$

and

$$S_{A,I}^{\mathrm{ref}I} = \sum \mathrm{PM}_{A,I}^{\mathrm{ref}I}\ ,\quad S_{B,I}^{\mathrm{ref}I} = \sum \mathrm{PM}_{B,I}^{\mathrm{ref}I}\ ,\quad (I = 1,2,3,\ldots,N)\ ,$$

are compared separately at each SNP locus, according to the concordance of the SNP calls in the tumor sample (O_i^{tum}) and the SNP calls in a given reference sample ($O_i^{\mathrm{ref}I}$),

$$R_{A,i}^{\mathrm{ref}I} = \frac{S_{A,i}^{\mathrm{tum}}}{S_{A,i}^{\mathrm{ref}I}} \qquad (\text{for } O_i^{\mathrm{tum}} = O_i^{\mathrm{ref}I}),$$

$$R_{B,i}^{\mathrm{ref}I} = \frac{S_{B,i}^{\mathrm{tum}}}{S_{B,i}^{\mathrm{ref}I}}$$

and the total CN ratio is calculated as follows:

$$R_{AB,i}^{\mathrm{ref}I} = \begin{cases} R_{A,i}^{\mathrm{ref}I} & \text{for } O_i^{\mathrm{tum}} = O_i^{\mathrm{ref}I} = AA \\ R_{B,i}^{\mathrm{ref}I} & \text{for } O_i^{\mathrm{tum}} = O_i^{\mathrm{ref}I} = BB \\ \frac{1}{2}\left(R_{A,i}^{\mathrm{ref}I} + R_{B,i}^{\mathrm{ref}I}\right) & \text{for } O_i^{\mathrm{tum}} = O_i^{\mathrm{ref}I} = AB \end{cases} \quad (I = 1,2,3,\ldots,N)\ .$$

For CN estimations, however, $R_{AB,i}^{\mathrm{ref}I}$, $R_{A,i}^{\mathrm{ref}I}$, and $R_{B,i}^{\mathrm{ref}I}$ are biased by differences in mean array signals and different PCR conditions between the tumor sample and each reference sample and need to be compensated for these effects to obtain their adjusted values $\hat{R}_{AB,i}^{\mathrm{ref}I}$, $\hat{R}_{A,i}^{\mathrm{ref}I}$, and $\hat{R}_{B,i}^{\mathrm{ref}I}$, respectively (appendix A).[16]

These values are next averaged over the references that have a concordant genotype for each SNP in a given set of references (K), and we obtain $\tilde{R}_{AB,i}^{K}$, $\tilde{R}_{A,i}^{K}$, and $\tilde{R}_{B,i}^{K}$. Note that $\tilde{R}_{A,i}^{K}$ and $\tilde{R}_{B,i}^{K}$ are calculated only for heterozygous SNPs in the tumor sample (see appendix A for more details).

A provisional total CN profile Λ_K is provided by

$$\Lambda_K = \{\tilde{R}_{AB,i}^{K}\}\ ,$$

and provisional AsCN profiles are obtained by

$$\Lambda_K^{\mathrm{large}} = \{\max(\tilde{R}_{A,i}^{K}, \tilde{R}_{B,i}^{K})\}$$

$$\Lambda_K^{\mathrm{small}} = \{\min(\tilde{R}_{A,i}^{K}, \tilde{R}_{B,i}^{K})\}\ .$$

These provisional analyses, however, assume that the tumor genome is diploid and has no gross CN alterations, when the coefficients are calculated in regressions. In the next step, the regressions are iteratively performed using a diploid region that is truly or is expected to be diploid, to determine the coefficients on the basis of the provisional total CN, and then the CNs are recalculated.

Finally, the optimized set of references is selected that minimizes the SD of total CN at the diploid region by stepwise reference selection, as described in appendix A.

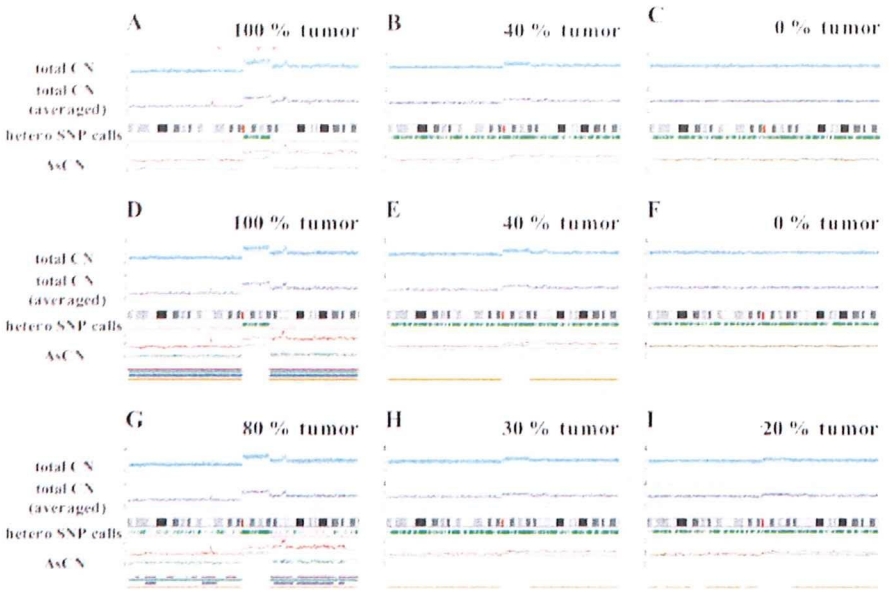

Figure 1. AsCN analysis with or without paired DNA. DNA from a lung cancer cell line (NCI-H2171) was mixed with DNA from an LCL (NCI-BL2171) established from the same patient at the indicated percentages and was analyzed with GeneChip 50K Xba SNP arrays. AsCNs, as well as total CNs, were analyzed using either the paired reference sample (NCI-BL2171) (*upper panels, A–C*) or samples from unrelated individuals simultaneously processed with the tumor samples (*middle and lower panels, D–I*). On each panel, the upper two graphs represent total CNs and their moving averages for the adjacent 10 SNPs, whereas moving averages of AsCNs for the adjacent 10 SNPs are shown below (*red and green lines*). Green and pink bars in the middle are heterozygous (hetero) calls and discordant SNP calls between the tumor and its paired reference, respectively. At the bottom of each panel, LOH regions inferred from AsCNAR (*orange*), SNP call–based LOH inference of CNAG (*blue*), dChip (*purple*), and PLASQ (*light green*) are depicted. Asterisks (*) indicate the loci at which total CNs were confirmed by FISH analysis (data not shown). The calibrations of CN graphs are linearly adjusted so that the mean CNs of null and single alleles should be 0 and 1, respectively.

Allele-specific analysis using a constitutive reference, refSelf, is provided by

$$\Lambda^{\text{large}} = \left\{\max\left(\hat{R}_{A,i}^{\text{refSelf}}, \hat{R}_{B,i}^{\text{refSelf}}\right)\right\}$$

and

$$\Lambda^{\text{small}} = \left\{\min\left(\hat{R}_{A,i}^{\text{refSelf}}, \hat{R}_{B,i}^{\text{refSelf}}\right)\right\} .$$

Computational details of AsCNAR are provided in appendix A.

Comparison with Other Algorithms

dChip[17] and PLASQ[18] were downloaded from their sites, and the identical microarray data were analyzed using these programs. Since PLASQ requires both Xba and Hind array data, microarray data of mixed tumor contents for Hind arrays were simulated by linearly superimposing the tumor cell line (NCI-H2171) and LCL (NCI-BL2171) data at indicated proportions.

Statistical Analysis

Significance of the presence of allelic imbalance (AI) in a given region, Γ, called as having AI by the hidden Markov model (HMM), was statistically tested by calculating t statistics for the difference in AsCNs, $|\log_2 \tilde{R}_{A,i}^{K} - \log_2 \tilde{R}_{B,i}^{K}|$, between Γ and a normal diploid region, where the tests were unilateral. Significance between the numbers of UPDs detected by the SNP call–based method and by AsCNAR was tested by one-tailed binominal tests. P values for AI detection by allele-specific PCR were calculated by one-tailed t tests, comparing triplicates of the target sample and triplicates of five normal samples that have heterozygous alleles in the SNP.

Detection of the JAK2 *Mutation and Measurements of Relative Allele Doses*

The *JAK2* V617F mutation was examined by a restriction enzyme–based analysis, in which PCR-amplified *JAK2* exon 12 fragments were digested with *Bsa*XI, and the presence of the undigested fragment was examined by gel electrophoresis.[5] Relative allele dose between wild-type and mutated *JAK2* was determined by measuring allele-specific PCR products for wild-type and mutated *JAK2* alleles by

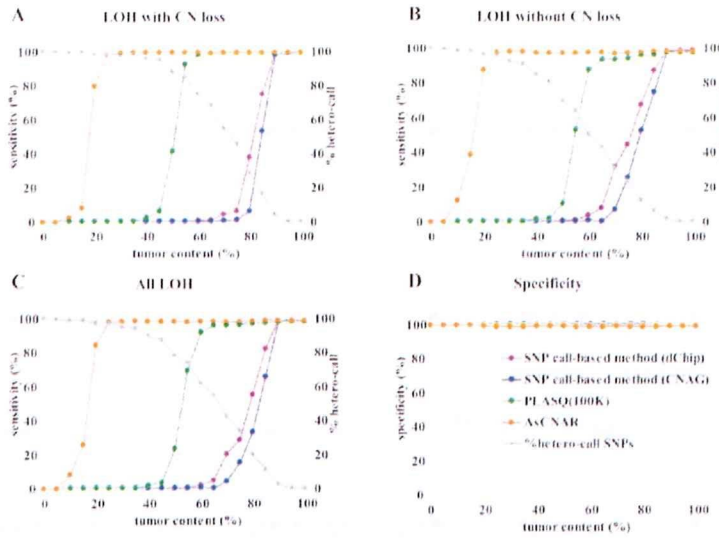

Figure 2. Sensitivity and specificity of LOH detection for intentionally mixed tumor samples. Sensitivity of detection of LOH with or without CN loss (*A* and *B*) in different algorithms were compared using a mixture of the tumor sample (NCI-H2171) and the paired LCL sample (NCI-BL2171). The results for all LOH regions are shown in panel C, and the specificities of LOH detection are depicted in panel D. For precise estimation of sensitivity and specificity, we defined the SNPs truly positive and negative for LOH as follows. The tumor sample and the paired LCL sample were genotyped on the array three times independently, and we considered only SNPs that showed the identical genotype in the three experiments. SNPs that were heterozygous in the paired LCL sample and were homozygous in the tumor sample were considered to be truly positive for LOH, and SNPs that were heterozygous both in the paired LCL sample and in the tumor sample were considered to be truly negative. Proportions of heterozygous SNP calls (%hetero-call) that remained in LOH regions of each sample are also shown in panels A–C.

capillary electrophoresis by use of the 3100 Genetic Analyzer (Applied Biosystems), as described in the literature.[19] Likewise, the fraction of tumor components having 9p and other UPDs was measured by either allele-specific PCR or STR PCR,[7,19] by use of the primers provided in appendix B [online only]. The percentage of UPD-positive cells (%UPD(+)) was also estimated as the mean difference of AsCNs for heterozygous SNPs within the UPD region divided by that for homozygous SNPs within an arbitrary selected normal region:

$$\%\mathrm{UPD}(+) = \frac{E(|\tilde{R}^K_{A,j} - \tilde{R}^K_{B,i}|_{i\in\text{hetero SNPs in UPD region}})}{E(|\tilde{R}^K_{A,j} - \tilde{R}^K_{B,j}|_{j\in\text{homo SNPs with normal CN}})},$$

where AsCNs for the denominator were calculated as if the homozygous SNPs were heterozygous. However, in those samples with a high percentage of UPD-positive components, the heterozygous SNP rate in the UPD region decreased. For such regions, we calculated the percentage of UPD-positive cells by randomly selecting 30% (the mean heterozygous SNP call rate for this array) of all the SNPs therein and by assuming that they were heterozygous SNPs. Cellular composition of *JAK2* wild-type (wt) and mutant (mt) homozygotes (wt/wt and mt/mt) and heterozygotes (wt/mt) in each MPD specimen was estimated assuming that all UPD components are homozygous for the *JAK2* mutation. The fractions of the wt/mt heterozygotes in cases with a 9p gain were estimated assuming that the duplicated 9p alleles had the *JAK2* mutation. Throughout the calculations, small negative values for wt/mt were disregarded.

FISH

FISH analysis was performed according to the previously published method, to confirm the absolute total CNs in NCI-H2171.[20] The genomic probes were generated by whole-genome amplification of FISH-confirmed RP11 BAC clones 169N13 (3q13; CN = 2), 227F7 (8q24; CN = 2), 196H14 (12q14; CN = 2), 25E13 (13q33; CN = 2), 84E24 (17q24; CN = 2), 12C9 (19q13; CN = 2), 153K19 (3q13; CN = 3), 94D19 (3p14; CN = 1), 80P10 (8q22; CN = 1), and 64C21 (13q12-13; CN = 1), which were obtained from the BACPAC Resources Center at the Children's Hospital Oakland Research Institute in Oakland, California.

Results

SNP Call–Based Genomewide LOH Detection by Use of SNP Arrays

When a pure tumor sample is analyzed with a paired constitutive reference on a GeneChip Xba 50K array, LOH is easily detected as homozygous SNP loci in the tumor spec-

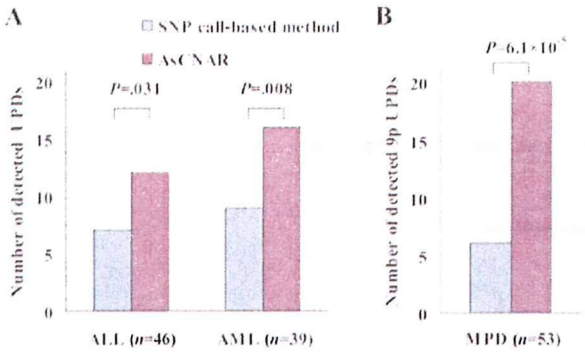

Figure 3. The number of UPD regions for acute leukemia and MPD samples detected by either the SNP call–based method or AsCNAR. The number of UPD regions for ALL and AML samples detected by the SNP call–based method or by AsCNAR is shown in panel A, and the number of 9p UPDs for MPD samples detected by the two methods is shown in panel B. Some samples have more than one UPD region. Details of UPD regions are given in table 1. Significance between the numbers of UPDs detected by the SNP call–based method and by the AsCNAR method was tested by one-tailed binomial tests.

imen that are heterozygous in the constitutive DNA (fig. 1*A*, pink bars). In addition, given a large number of SNPs to be genotyped, the presence of LOH is also inferred from the grossly decreased heterozygous SNP calls, even in the absence of a paired reference (fig. 1*D*). The accuracy of the LOH inference would depend partly on the algorithm used but more strongly on the tumor content of the specimens. Thus, our SNP call–based LOH inference algorithm in CNAG (appendix C), as well as that of dChip,[17] show almost 100% sensitivity and specificity for pure tumor specimens. But, as the tumor content decreases, the LOH detection rate steeply declines (fig. 1*G*), and, with <50% tumor cells, no LOH can be detected, even when complete genotype information for both tumor and paired constitutive DNA is obtained (fig. 1*B*, 1*E*, 1*H*, and 1*I*).

LOH Detection Based on AsCN Analysis

On the other hand, the capability of allele-specific measurements of CN alterations in cancer genomes is an excellent feature of the SNP array–based CN-detection system that uses a large number of SNP-specific probe sets.[16,18,21] When constitutive DNA is used as a reference, AsCN analysis is accomplished by separately comparing the SNP-specific array signals from the two parental alleles at the heterozygous SNP loci in the constitutive genomic DNA.[16] It determines not only the total CN changes but also the alterations of allelic compositions in cancer genomes, which are captured as the split lines in the two AsCN graphs (fig. 1*A* and 1*B*). In this mode of analysis, the presence of LOH can be detected as loss of one parental allele, even in specimens showing almost no discordant calls (fig. 1*B*).

AsCNAR

The previous method for AsCN analysis, however, essentially depends on the availability of constitutive DNA, since AsCNs are calculated only at the heterozygous SNP loci in constitutive DNA.[16] Alternatively, allele-specific signals can be compared with those in anonymous references on the basis of the heterozygous SNP calls in the tumor specimen. In the latter case, the concordance of heterozygous SNP calls between the tumor and the unrelated sample is expected to be only 37% with a single reference. However, the use of multiple references overcomes the low concordance rate with a single reference, and the expected overall concordance rate for heterozygous SNPs and for all SNPs increases to 86% and 92%, respectively, with five unrelated references (appendix D [online only]). Thus, for AsCNAR, allele-specific signal ratios are calculated at all the concordant heterozygous SNP loci for individual references, and then the signal ratios for the identical SNPs are averaged across different references over the entire genome. For the analysis of total CNs, all the concordant SNPs, both homozygous and heterozygous, are included in the calculations, and the two allele-specific signal ratios for heterozygous SNP loci are summed together. Since AsCNAR computes AsCNs only for heterozygous SNP loci in tumors, difficulty may arise on analysis of an LOH region in highly pure tumor samples, in which little or no heterozygous SNP calls are expected. However, as shown above, such LOH regions can be easily detected by the SNP call–based algorithm, where AsCNAR is formally calculated assuming all the SNPs therein are heterozygous. Thus, the AsCNAR provides an essentially equivalent result to that from AsCN analysis using constitutional DNA, with similar sensitivity in detecting AI and LOH (compare fig. 1*A* with 1*D* and 1*B* with 1*E*).

As expected from its principle, AsCNAR is more robust in the presence of normal cell contaminations than are SNP call–based algorithms. To evaluate this quantitatively, we analyzed tumor DNA that was intentionally mixed with its paired normal DNA at varying ratios in 50K Xba SNP arrays, and the array data were analyzed with AsCNAR. To preclude subjectivity, LOH regions were detected by an HMM-based algorithm, which evaluates difference in AsCNs in both parental alleles (appendix E).[22] As the tumor content decreases, the SNP call–based LOH inference fails to detect LOH because of the appearance of heterozygous SNP calls from the contaminated normal cell component (fig. 1*E* and 1*G*–1*I*), but these heterozygous SNP calls, in turn, make AsCNAR operate effectively.

Table 1. CN-Neutral LOH in Primary Acute Leukemia

The table is available in its entirety in the online edition of *The American Journal of Human Genetics*.

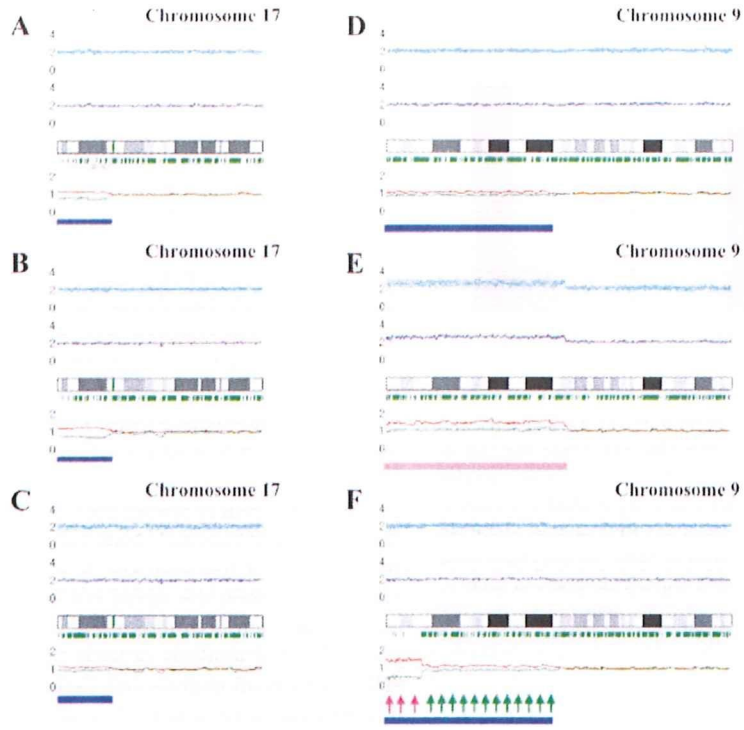

Figure 4. Detection of AI in samples of primary AML and MPD. AsCN analyses disclosed the presence of a small population with 17p UPD in a primary AML specimen (W150673) (93% blasts in microscopic examination) with either a paired sample (*A*) or anonymous reference samples (*B*). The difference of the mean CNs of the two parental alleles is statistically different between panels A (0.38) and B (0.55) ($P < .0001$, by t test), which is explained by the residual tumor component within the bone marrow sample in complete remission (1% blast) used as a paired reference (W150673CR) (*C*). AI in the 9p arm was also sensitively detected in *JAK2* mutation–positive MPD cases. UPD may be carried only by a very small population (~20% estimated from the mean deviation of AsCNs in 9p) (IMF_10) (*D*), or by two discrete populations within the same case (PV_06), as indicated by two-phased dissociation of AsCN graphs (*pink and green arrows*) (*F*). AI in 9p is mainly caused by UPD but may be caused by gains of one parental allele without loss of the other allele (*E*), both of which are not discriminated by conventional allele measurements. Blue and pink bars are UPD and AI calls, respectively, from the HMM-based LOH detection algorithm. Other features are identical to those indicated in figure 1.

In fact, this algorithm precisely identifies known LOH regions, as well as regions with AI, in intentionally mixed tumor samples containing as little as 20% (for LOH without CN loss) to 25% (LOH with CN loss) tumor contents (fig. 2*A*–2*C*). Note that this large gain in sensitivity is obtained without the expense of specificity, which is very close to 100%, as observed with other algorithms (fig. 2*D*). In AsCNAR, small regions of AI (<1 million bases in length) are difficult to detect in samples contaminated with normal cells. However, such regions are also difficult to detect using other algorithms (data not shown).

Identification of UPD in Primary Tumor Samples

To examine further the strength of the newly developed algorithms for AsCN and LOH detection, we explored UPD regions in 85 primary acute leukemia samples, including 39 AML and 46 ALL samples, on GeneChip 50K Xba SNP arrays, since recent reports identified frequent (~20%) occurrence of this abnormality in AML.[23,24] In the SNP call–based LOH inference algorithm, 16 UPD regions were identified in 14 cases, 8 (20.5%) AML and 6 (13.0%) ALL. However, the frequencies were almost doubled with the AsCNAR algorithm; a total of 28 UPD loci were identified in 25 cases, including 14 (35.9%) AML and 11 (23.9%) ALL (fig. 3*A* and table 1). In 5 of the 25 UPD-positive cases, a matched remission sample was available for AsCN analysis, which provided essentially the same results as AsCNAR, except for one relapsed AML case (W150673). In the latter case, a discrepancy in AsCN shifts in 17p UPD occurred between AsCN analysis with and without a constitutive reference, with more CN shift detected with anonymous references (fig. 4*A* and 4*B*). The discrepancy was, however, explained by the unexpected detection of a subtle UPD change in 17p in the reference sample by

Table 2. AI of 9p in *JAK2* Mutation-Positive MPDs

Case	9p Status by AsCNAR			Detection by SNP Call–Based Method[c]	% *JAK2* Mutation[b]	Allele-Specific PCR[e]		
	Type	Break Point[d]	%UPD[e]			SNP	%UPD[f]	*P*[g]
PV_02	Gain	42.9	99	NA	63	*rs2009991*	84	.004
PV_03	Gain	Whole	60	NA	39	*rs10511431*	63	.008
PV_04	UPD	37.0	93	D	95	5Homo	5Homo	5Homo
PV_08	UPD	34.2	91	D	93	5Homo	5Homo	5Homo
PV_07	UPD	23.8	88	D	90	5Homo	5Homo	5Homo
PV_06	UPD[h]	7.1/35.3	83	D	93	5Homo	5Homo	5Homo
PV_11	UPD	31.2	68	D	76	5Homo	5Homo	5Homo
PV_13	UPD	28.1	66	ND	48	*rs1416582*	64	.001
PV_01	UPD	20.9	56	ND	62	*rs10511431*	49	.007
PV_09	UPD	30.8	38	ND	30	*rs10491558*	32	.020
PV_05	UPD	23.5	32	ND	33	*rs1374172*	31	.010
IMF_04	UPD	33.8	79	D	90	5Homo	5Homo	5Homo
IMF_05	UPD	37.0	58	ND	57	*rs1416582*	49	.004
IMF_07	UPD	20.3	52	ND	50	*rs1416582*	57	.005
IMF_12	UPD[h]	26.8/42.9	52	ND	66	5Homo	5Homo	5Homo
IMF_14	UPD[h]	22.8/33.8	45	ND	56	*rs1374172*	35	.015
IMF_19	UPD	34.4	26	ND	43	*rs10511431*	33	.017
IMF_10	UPD	34.6	21	ND	36	*rs1374172*	21	.049
IMF_15	UPD	33.8	21	ND	17	*rs10511431*	20	.084
IMF_06	UPD	35.3	17	ND	28	*rs1374172*	20	.048
IMF_16	(−)	NA	NA	NA	37	NA	NA	NA
ET_12	Gain	Whole	42	NA	27	*rs2009991*	36	.046
ET_14	UPD	42.9	63	ND	45	*rs1374172*	54	.006
ET_01	UPD	35.4	19	ND	59	*rs10511431*	33	.017
ET_05	(−)	NA	NA	NA	23	NA	NA	NA
ET_08	(−)	NA	NA	NA	42	NA	NA	NA
ET_09	(−)	NA	NA	NA	34	NA	NA	NA
ET_10	(−)	NA	NA	NA	16	NA	NA	NA
ET_15	(−)	NA	NA	NA	27	NA	NA	NA
ET_18	(−)	NA	NA	NA	17	NA	NA	NA
ET_19	(−)	NA	NA	NA	27	NA	NA	NA
ET_21	(−)	NA	NA	NA	55	NA	NA	NA

NOTE.—NA = not applied; (−) = neither UPD nor gain of 9p was detected by AsCNAR analysis.

[c] D = UPD was detected by SNP call–based method; ND = not detected.

[b] Percentage of *JAK2* mutant alleles, as measured by allele-specific PCR.

[e] 5Homo = all five tested SNPs were homozygous.

[d] Position of the break point from the p-telomeric end (values are in Mb). The location of *JAK2* corresponds to 5 Mb.

[e] Percentage of tumor cell populations with either UPD or gain of 9p, as determined by AsCNAR analysis.

[f] Percentage of tumor cell populations with either UPD or gain of 9p, as determined by the allele-specific PCR.

[g] *P* values were derived from one-tailed *t* tests comparing triplicate analyses of the target sample and triplicate analyses of five normal samples.

[h] Two UPD-positive populations exist.

AsCNAR ($P < .0001$, by t test) (fig. 4*C*), which offset the CN shift in the relapsed sample, although it was morphologically and cytogenetically diagnosed as in complete remission.

Analysis of 9p UPD in MPDs

Another interesting application of the AsCNAR is the analysis of allelic status in the 9p arm among patients with MPD, which includes PV, ET, and IMF. According to past reports, ~10% (in ET) to ~40% (in PV) of MPD cases with the activating *JAK2* mutation (V617F) show evidence of clonal evolution of dominant progeny that carry the homozygous *JAK2* mutation caused by 9p UPD.[5,7,8] In our series that included 53 MPD cases, the *JAK2* mutation was detected in 32 (60%), of which 13 (41%) showed >50% mutant allele by allele measurement with the use of allele-specific PCR, and thus were judged to have one or more populations carrying homozygous *JAK2* mutations (table 2). This frequency is comparable to that reported elsewhere.[8] However, when the same specimens were analyzed with 50K Xba SNP arrays by use of the AsCNAR algorithm, 20 of the 32 *JAK2* mutation–positive cases were demonstrated to have minor UPD subpopulations (table 2 and fig. 3*B*), in which as little as 17% of UPD-positive populations were sensitively detected (fig. 4*D*). In fact, these minor (<50%) UPD-positive populations in these